Influence of bloom dynamics on Particle Export Efficiency in the North Atlantic: a comparative study of radioanalytical techniques and sediment traps

E. Ceballos-Romero[1]*, F.A.C. Le Moigne[3, 2], S. Henson[2], C.M. Marsay[4, †], R.J. Sanders[2], and R. García-Tenorio[1], M. Villa-Alfageme[1]

[1] Dpto. Física Aplicada II. Universidad de Sevilla. Av. Reina Mercedes, 2. 41012 Sevilla, Spain

[2]Ocean Biogeochemistry and Ecosystems, National Oceanography Centre, Southampton, SO14 3ZH, UK

[3]GEOMAR Helmholtz Centre for Ocean Research Kiel, Düsternbrooker Weg 20, D-24105 Kiel, Germany

[4]Ocean and Earth Science, National Oceanography Centre Southampton, University of Southampton, Southampton, SO14 3ZH, United Kingdom.

[†]Now at: Skidaway Institute of Oceanography, University of Georgia, 10 Ocean Science Circle, Savannah, GA 31411, USA

*Corresponding author: E. Ceballos-Romero, email: elecebrom@alum.us.es,

Keywords: POC export flux, primary production, PELAGRA sediment trap, ^{234}Th, ^{210}Po, particle export efficiency, Irminger Basin, Iceland Basin

Abstract

The Biological Carbon Pump is an important component of the global carbon cycle is (BCP). Particle Export Efficiency (PE_{eff}), defined as the proportion of primary production (PP) exported as Particulate Organic Carbon (POC) from the surface ocean, is increasingly used as a metric of the strength of the BCP. However our knowledge of which factors drive variability of PE_{eff} remains poor. This is partially because comparisons of PE_{eff} in different regions often overlook the timescale over which the method used operates in relation to the phase of the plankton bloom. Here we use three techniques to estimate PE_{eff} *in situ* in the North Atlantic: the radioactive pairs ^{238}U-^{234}Th and ^{210}Pb-^{210}Po, and neutrally buoyant sediment traps (PELAGRA).

Order of magnitude discrepancies between values of PE_{eff} obtained from PELAGRA relative to those obtained when applying both radionuclide techniques. POC export fluxes and satellite-derived PP suggest that this results from the differing time scales covered by the three methods and the timing of observations relative to the bloom peak. None of the three techniques are considered inappropriate to estimate PE_{eff} *in situ*, but bloom dynamics must be considered in relation to the duration over which a particular sampling method operates.

Our results suggest a strong seasonal variability in PE_{eff}, most likely controlled by the community structure and hydrographic conditions. This implies that the methods used (specifically their inherent timescales) and the phase of the bloom at the time of sampling must be carefully taken into account to ensure that individual PE_{eff} estimates compiled from different sources to construct global export algorithms are comparable.

1. Introduction

The Biological Carbon Pump (BCP) is an important component of the marine carbon cycle (Volk and Hoffert, 1985). The BCP removes CO_2 from the atmosphere by the coupling of production and export processes. Large amounts of organic carbon are transferred from the upper ocean to the ocean's interior through the sinking of biogenic particles constituting a complex mix of biogeochemical material. Without the BCP atmospheric CO_2 concentration relative to preindustrial levels would be ~50 % higher than it currently is (Parekh et al., 2006; Sanders et al., 2014). Hence, quantifying the efficiency with which the BCP removes carbon from the upper ocean on both global and regional scales is fundamental for understanding the carbon cycle. A small fraction of particulate organic carbon (POC) generated through primary production (PP) in surface waters survives respiration and leaves the mesopelagic zone, but most of this sinking POC flux is remineralised on its way to the ocean bottom due to the combined action of bacteria and zooplankton (Giering et al.,

2014). Ducklow et al., 2002 and Poulton et al., 2006 estimated that only around 1% of the total surface PP reaches the seafloor.

One metric for the strength of the BCP is the Particle Export Efficiency, PE_{eff}, defined as POC export from the surface layer as a fraction of PP. In this study, PE_{eff} is estimated approximately at 150m (i.e. flux at 150 m relative to PP) and the reference surface layer is 10 m depth. PE_{eff} is mainly controlled by *(i)* the level of primary production (De La Rocha and Passow, 2007); *(ii)* the sinking velocity of particles carrying organic carbon (De La Rocha and Passow, 2007); *(iii)* the rate of surface remineralisation (Le Moigne et al., 2016); *(iv)* the ballast content of particles (Banse, 1990; De La Rocha and Passow, 2007; Le Moigne et al., 2014b); and (*v)* the variability in zooplankton abundance and therefore grazing (Cavan et al., 2015; Le Moigne et al., 2015). However the way these variables shape the seasonal and spatial variability of the strength of the BCP (Henson et al., 2015, 2011; Kwon et al., 2009) remain imprecisely constrained.

Currently, radionuclide techniques (Buesseler et al., 1998; Le Moigne et al., 2013a; Le Moigne et al., 2013b; Rutgers Van Der Loeff et al., 1997; Stewart et al., 2007; Verdeny et al., 2009), and neutrally buoyant traps (Buesseler et al., 2008b; Lamborg et al., 2008; Lampitt et al., 2008; Marsay et al., 2015; Owens et al., 2013; Peterson et al., 2009; Valdes and Price, 2000) are widely used to estimate particle export *in situ*, while other methods such as the marine snow catcher (Cavan et al., 2015; Riley et al., 2012) provide additional information (e.g. particle sinking speed and pellet flux). ^{234}Th and ^{210}Po isotope tracers are commonly used to estimate export since their half-lives (24.1 days and 138.4 days respectively) and particle affinities make them suitable to assess POC export from the surface ocean (Bacon et al., 1976; Cochran et al., 1993; Stewart et al., 2011; van der Loeff and Geibert, 2008; Verdeny et al., 2009; Villa-Alfageme et al., 2014). Due to their different biogeochemical behaviours relative to their parent isotopes (^{238}U and ^{210}Pb), ^{234}Th and ^{210}Po are scavenged onto particles and removed from the surface ocean as those particles sink. The export flux of radionuclide is directly obtained from the radioactive disequilibrium between parent and daughter,

and is converted into POC export by using the POC:radionuclide (*POC:R*) ratio measured on sinking particles. Neutrally buoyant sediment traps directly measure the amount of material settling down through the water column in order to estimate POC flux, with one design being PELAGRA (Particle Export measurement using a LAGRAngian trap; Lampitt et al. (2008)).

The methods employed for the study of PE_{eff} do not always provide consistent estimates of carbon export and the differences between approaches are generally overlooked when interpreting results. For instance, using *in situ* observations from the ^{234}Th technique (Henson et al., 2011), or from the *f*-ratio (Laws et al., 2000), combined with satellite-derived SST and PP data yielded estimates of export flux for the North Atlantic ranging from 0.5-1.7 Gt C yr^{-1} (Sanders et al., 2014). In contrast using sediment traps, Antia et al. (2001) estimated values of 1.3 Gt C yr^{-1} in this region. Not many studies have compared radionuclide techniques traps simultaneously with the exception of Le Moigne et al. (2013b) (neutrally buoyant PELAGRA traps, ^{234}Th and ^{210}Po), Stewart et al. (2007a) (moored sediment traps, ^{234}Th and ^{210}Po), Buesseler et al. (2008a) (VERTEX style sediment traps, ^{234}Th and ^{210}Po), and Stewart et al. (2011) (cylindrical traps, ^{234}Th and ^{210}Po), who carried out studies at the Porcupine Abyssal Plain (PAP) site, Bermuda Atlantic Time-series Study (BATS), Mediterranean Sea (MedFlux project) and Sargasso Sea (BATS) respectively. Le Moigne et al. (2013b) and Stewart et al. (2011) found that ^{234}Th-derived POC fluxes were systematically higher than ^{210}Po-derived fluxes during low flux periods, and higher or similar to those measured in traps within the euphotic zone (E_z), while Stewart et al. (2007a) found the same behaviour below the E_z through three seasons (early spring, late spring, summer). In contrast Buesseler et al. (2008a) reported higher ^{210}Po-derived fluxes than ^{234}Th-derived POC fluxes and traps (which were in good agreement). Such discrepancies highlight the need for a thorough examination of the variables affecting PE_{eff} estimates when using these techniques in order to guarantee their correct application and interpretation.

Here we present a comparison of downward POC fluxes obtained from the simultaneous use of the three methods, PELAGRA, ^{234}Th and ^{210}Po, in the Irminger Basin (IRB) and the Iceland Basin (IB), during summer 2010. In addition, we compare our results to PE_{eff} estimates derived from three other studies in the North Atlantic in which at least one of the three techniques examined here was used. These studies took place in the IRB and IB in spring 2010, and at the Porcupine Abyssal Plain (PAP Site) in both spring 2012 (Villa-Alfageme et al., 2016) and summer 2009 (Le Moigne et al., 2013b). We aim to *(i)* assess the influence of the technique used on PE_{eff} estimates and obtain new insights into the interpretation of PE_{eff} estimates from different techniques given their different timescales of coverage; *(ii)* examine the variability of PE_{eff} in different bloom phases.

2. Methods and sampling

2.1. Study area

The North Atlantic is known for its highly productive waters (Sanders et al., 2014). Spring blooms are thought to be very efficient at exporting POC and transferring it through the mesopelagic (Sanders et al., 2014). Annually, averaged satellite-derived export efficiency of ~10-15% is high relative to the 5% observed in the oligotrophic North Atlantic (Henson et al., 2012; Siegel et al., 2014).

The IRB and IB are oceanic basins located in the High Latitude North Atlantic (HLNA) (Figure 1) defined as the areas north of 58°N with a depth of >1000 m and, respectively, west and east of the Reykjanes Ridge (Gómez-Guzmán et al., 2013). The IRB and IB have a transient spring period of high biomass and hence high productivity and export (Nielsdóttir et al., 2009). However, despite shallow mixed layers, residual nitrate conditions are found in summer in the IB due to iron limitation that contributes to incomplete utilization of surface macronutrients (Le Moigne et al., 2014a; Sanders et al., 2005), which highlights an inefficiency of the biological carbon pump (Le Moigne et al., 2014a; Nielsdóttir et al., 2009; Sarmiento and Toggweiler, 1984).

The PAP site is located within the North Atlantic Drift-province (NADR) at 48.83°N, 16.5°W (Le Moigne et al., 2013b), at the boundary between the sub-polar and sub-tropical gyres of the North Atlantic (Henson et al., 2009). The PAP site is characterized by a strong spring bloom in April-May (Painter et al., 2010). A comprehensive summary of the hydrography, meteorology and upper mixed layer dynamics of the region can be found in Lampitt et al. (2001).

Both IRB and IB were visited twice in 2010 during cruises on board RRS *Discovery*: a spring cruise (D350) from 26th of April to the 9th of May (Day Of Year (DOY) 116-129), and a summer cruise (D354) from 4th July to 11th August (DOY 185-223) (details in Table 1). A total of 7 stations distributed over both basins were sampled for ^{234}Th-derived POC fluxes as part of cruise D350 (Figure 1), which coincided with the eruption of the Icelandic Eyjafjallajökull volcano (DOY 104-142, Achterberg et al. (2013)). Later, 15 stations were occupied for ^{234}Th and ^{210}Po during cruise D354 (Figure 1), which also involved 4 deployments of PELAGRA traps split between the two basins (details in Table 2.) Radionuclide samples were collected from a stainless steel CTD rosette.

Sampling during the PAP cruises followed a similar methodology and is detailed in (Villa-Alfageme et al., 2016) and Le Moigne et al. (2013b). The PAP Site was sampled in summer 2009 as part of cruise D341 on board RRS *Discovery*. A total of 10 and 9 stations were respectively sampled for ^{234}Th and ^{210}Po analysis, and 3 PELAGRA deployments were carried out during DOY 194 and 220. In spring 2012, cruise JC071 on board RRS *James Cook* sampled PAP site for ^{210}Po-derived POC fluxes between DOY 122 and 129 (Villa-Alfageme et al., 2016). Details of both cruises are given in Table 1.

2.2. Total water ^{234}Th analysis

Water samples (4L) were collected for ^{234}Th analysis at 10 depth horizons from the surface to 500 m (details are shown in Table S1 and S2). Measurement of total ^{234}Th was based on the MnO_2 precipitation method (Pike et al., 2005; Rutgers Van Der Loeff et al., 1997) in which ^{234}Th, together

153 with other radionuclides, is scavenged while its parent ^{238}U is left in the dissolved phase. Seawater
154 samples were acidified to pH = 1-2 with concentrated HNO_3, and spiked with ^{230}Th as a yield
155 monitor. After 6 hours to allow for homogenization, 7-8 ml of NH_4OH (pH up to 8-8.1) were added.
156 A MnO_2 precipitate was formed by the addition of 50 µL of $KMnO_4$ (7.5 g/L), followed by 50 µL of
157 $MnCl_2$ (7.5 g/L). Samples were shaken between each addition and allowed to stand and settle for 12
158 hours before being filtered onto 25 mm pre-combusted QMA filters. Finally, filters were dried at
159 60ºC for 24 hours, wrapped in Mylar and aluminium foil and then counted at sea for beta activity of
160 the high-energy daughter, ^{234}Pa in a Riso beta counter (Buesseler et al., 2008b; Morris et al., 2007).
161 Extraction efficiencies for ^{234}Th were 90.6 ± 6.7% (Le Moigne et al., 2014a, 2013a). Beta counter
162 calibration was carried out in the water column using deep water samples collected from > 1000m
163 (Morris et al., 2007). Corrections were made for ^{234}Th decay and ^{234}Th in growth from ^{238}U decay. In
164 addition, background corrections that included long-lived beta impurities were made following
165 repeated counting after 6-months (> 6 ^{234}Th half-lives). For the ^{234}Th recovery measurement a double
166 spike technique was used. Filtered precipitates were dissolved with H_2O_2 and HNO_3 and an internal
167 standard of ^{229}Th was added as recommended by GEOTRACES protocol (Maiti et al., 2012).
168 Samples were purified using anion-exchange chromatography and $^{230}Th/^{229}Th$ ratios were measured
169 by ICP-MS to determine the recoveries (Pike et al., 2005).
170 The ^{238}U results were obtained from calibrated salinity measurements. ^{238}U activity (A_U, dpm kg^{-1})
171 was calculated as $A_U = 0.0686 \times$ salinity (Chen et al., 1986), with a salinity value of 35 used.
172
173 *2.3. Total water ^{210}Pb and ^{210}Po analysis*
174 For ^{210}Po-^{210}Pb analysis, 5L water samples were collected from 10 to 13 depths between 0-1000 m.
175 The sampling distribution was focused between 0 and 500 m, where the most significant
176 disequilibrium between ^{210}Po and ^{210}Pb is expected (details in Table S3). We followed the
177 radiochemical procedure detailed in Le Moigne et al. (2013b), as well as the recommendations given

178 in the GEOTRACES protocol (Baskaran et al., 2013; Church et al., 2012). Seawater samples
179 (5L) were acidified to pH = 2, spiked with radioactive ^{209}Po ($T_{1/2}$ = 102 y) and stable Pb^{2+} as yield
180 tracers, and Fe^{3+} carrier. After 6 hours of equilibration, the pH was adjusted to 8.5 by adding NH_4OH
181 to allow $Fe(OH)_3$ to co-precipitate and settle ^{210}Pb and ^{210}Po. The supernatant was carefully removed
182 via siphoning, and the precipitate transferred to 250-mL bottles and stored for later treatment. The
183 consequent radiochemical analysis of these samples was undertaken at CITIUS (Centro de
184 Investigación, Tecnoligía e Innovación de la Universidad de Sevilla, Spain) within less than two
185 months after sampling. In order to isolate ^{210}Po for alpha counting measurement, radiochemical
186 purification of polonium was conducted. Iron hydroxide was re-dissolved in 1M HCl, and Fe^{3+} was
187 reduced to Fe^{2+} by adding ascorbic acid. Polonium was heated (80 ºC) and stirred for at least 8 hours
188 allowing its self-deposition onto a silver disk, subsequently measured for ^{210}Po determination. Stable
189 Pb^{2+} aliquots were then taken for subsequent ^{210}Pb yield determination (Baskaran et al., 2013). A
190 second plating was performed to clean ^{209}Po and ^{210}Po from the initial solution (Church et al., 2012).
191 For ^{210}Pb determination, samples were stored for at least 6 months to allow for ^{210}Po in-growth from
192 dissolved ^{210}Pb and to allow determination of ^{210}Pb by a second self-deposition of ^{210}Po, following
193 the same procedure described above. To avoid potential bias in the recovery evaluation, we add ^{209}Po
194 as second spike in concentrations an order of magnitude higher than the on-board ^{209}Po spike. This
195 way the effect of the traces ^{209}Po left in the solution after the cleaning becomes negligible.
196 ^{210}Po samples were counted for alpha activity using Canberra PIPS detectors. ^{210}Pb yield was
197 determined through measurement of stable Pb by ICP-MS. Averaged extraction efficiencies for ^{210}Pb
198 were 95.9 ± 8.6%. ^{210}Po yield was determined using radioactive ^{209}Po as internal tracer. Extraction
199 efficiencies for ^{210}Po averaged 66.4 ± 1.2%. ^{210}Po and ^{210}Pb results were obtained by applying the
200 following corrections: detector background counts, and reagent contamination blanks for both ^{210}Po
201 and ^{210}Pb. ^{210}Pb activity was inferred from the second measurement of ^{210}Po after the subsequent
202 decay corrections to the separation date first and to the sampling date afterwards. ^{210}Po uncertainties

arise from the uncertainty associated with the internal tracer method, namely uncertainties in the counting of ^{209}Po (1%), ^{210}Po (5%), and ^{209}Po tracer (3%), and from the uncertainty associated with the measurement of ^{210}Pb after 6 months (7%). Decay corrections were also done to both ^{210}Pb and ^{210}Po before obtaining their activity concentrations in water. The corrections included were: decay of *in situ* ^{210}Pb between the sampling and the second plating for ^{210}Pb results; decay of ^{209}Po yield tracer from the time of last calibration to plating; decay of ^{210}Po and in-growth of ^{210}Po from *in situ* ^{210}Pb during the different steps of the procedure (Baskaran et al., 2013).

2.4. Sampling and analysis of particulate matter using Stand Alone Pumping Systems

To estimate the POC export, POC to particulate ^{234}Th(^{210}Po) ratios (POC:Th(Po) hereafter, in µmol dpm^{-1}) must be measured. Seven and 15 deployments of *in situ* pumps (Stand Alone Pumping Systems–SAPS, Challenger Oceanic ®) were respectively made, with two particle size classes - small (1-53 µm) and large (>53 µm) - determined by filtering large volumes of sea water (>500 L) through 53 µm and 1 µm NITEX® nylon mesh filters (293mm diameter) loaded in Challenger Oceanic filter holders (see Bishop et al. (2012) for a review of large volume in situ filtration methods). Pumps were deployed at each station for ^{234}Th and ^{210}Po derived carbon fluxes at 10 and 110 m below the mixed layer (MLD) as defined visually from the CTD displays, and in some stations at 400 m (stations 20, 22, 28 and 33). The deployments depths for SAPS will be discussed in section 4. More details can be found in section 4.1. Deployment depths ranged between 40-60 m (MLD + 10) and 140-200 m (MLD + 110) and were typically 50 m and 150 m respectively. A full description of SAPS deployments is shown in Tables S4 and S5).

Particles collected on the mesh were resuspended in filtered seawater (0.2 µm GF/F filters) and quantitatively split for subsequent measurements using a Folsom® splitter (1/4 for POC, 1/4 for ^{234}Th, 1/4 for ^{210}Po, 1/4 for other parameters not considered here). One split was filtered onto pre-combusted 25 mm GF/F filters and stored frozen for subsequent POC analysis as described in

228 Poulton et al. (2006). Splits for ^{210}Po and ^{234}Th analysis were filtered onto 25 mm GF/F and GMA
229 filters respectively.
230 ^{234}Th activity on QMA filters was measured on board. ^{210}Po and ^{210}Pb samples, both on 53 µm and
231 1-53 µm size fractions were fully digested in a mixture of 65% HNO_3, 37% HCl and 40% HF acids
232 and dried following a similar procedure as for the analysis of seawater samples (see section 2.3).
233
234 *2.5. ^{234}Th and ^{210}Po export flux calculation*
235 ^{234}Th and ^{210}Po downward fluxes (P) were calculated using a steady state one-box model described in
236 detail elsewhere (Buesseler et al., 1998; Savoye et al., 2006). Briefly, steady state (SS) conditions are
237 assumed (i.e. ^{234}Th and ^{210}Po concentrations are constant over time), and physical processes- such as
238 advection and/or upwelling- and a contribution of atmospheric ^{210}Po flux are ignored. The flux of
239 ^{234}Th and ^{210}Po (dpm m^{-2} d^{-1}) were calculated by integrating to a given depth (z = h = MLD + 110 m;
240 typically 150 m) as,

241 $$P^{SS} = \lambda \cdot \int_{z=0}^{z=h} (A_2 - A_1) \cdot dz \quad (1)$$

242 Experimental flux must be obtained from experimental discrete data points as,

243 $$P^{SS} = \sum_{z=0}^{z=h} (A_2 - A_1) \cdot dz \quad (2)$$

244 Where A_1 is the total ^{234}Th or ^{210}Po activity concentration (dpm m^{-3}), A_2 is the total parent activity
245 concentration (dpm m^{-3}) for ^{238}U or ^{210}Pb, and λ is the decay constant of the daughter element (d^{-1}).
246 To calculate the ^{234}Th- and ^{210}Po-derived POC fluxes, vertical ^{234}Th and ^{210}Po fluxes are used,
247 together with a conversion factor (*POC:R),* as:

248 $$POC_{flux}\ (mmol\ m^{-2} d^{-1}) = POC{:}R \cdot P^{SS} \quad (3)$$

249 where *POC:R* is the ratio POC to ^{234}Th or ^{210}Po (µmol dpm^{-1}), measured in sinking particles using
250 SAPS or PELAGRA at the corresponding integration depth (see sections 2.4, 2.6 and 4.1 for
251 discussion) and P is the integrated ^{234}Th or ^{210}Po flux (dpm m^{-2} d^{-1}) obtained from Equation 1.
252 Uncertainties for all individual measurements were obtained by error propagation of all the variables

included in the formulas (1) and (2). Both radionuclide fluxes and *POC:R* ratios contribute similarly to the total uncertainty. In the case of averaged values, uncertainties given correspond to one standard deviation (SD) of the values averaged.

2.6. PELAGRA drifting sediment traps. POC fluxes and POC:R ratios

The PELAGRA sediment trap is built around an APEX float (Webb Research Corporation, USA; Lampitt et al. (2008)). It is a neutrally buoyant platform with active buoyancy control to maintain the instrument at a level of constant pressure or density. Horizontal flow of particles across the collection funnels is presumed to be negligible owing to the fact that the trap is neutrally buoyant (Lampitt et al., 2008; Salter et al., 2007). During this cruise, PELAGRA traps were deployed at approximately 80, 150 and 400 m in both the IRB and IB (Figure 1 and Table 2). Limitations on sampling strategy derived from storm damage incurred during transit of cruise D354 along with technical problems with the shallower (typically 80 m) traps. A full description of the deployment strategy and analysis procedures used during cruise D354 can be found in Marsay (2012).

PELAGRA were used to directly measure POC fluxes (Marsay, 2012). Additionally, POC:Th(Po) ratios were estimated during this work for particles collected by PELAGRA. To do this, splits from the trap samples were analysed for ^{234}Th, ^{210}Po and POC in a similar way to that described in section 2.4 to obtain *POC:R* (Equation 3) for the sinking material.

2.7. Satellite data

Chlorophyll *a* concentration (Chl-*a*) data from the NASA MODIS satellite at 9 km, 8 day resolution were downloaded from http://oceancolor.gsfc.nasa.gov/. A time series of Chl-*a* for each station was created by averaging pixels within a 25 km radius of the sampling location. Chl-*a* concentration was converted to PP using the VGPM algorithm (Behrenfeld and Falkowski, 1997) in a consistent way as done in Henson et al. (2013). Both PP and Chl-*a* data are used to assess the bloom phase at the time

of sampling and as input to calculate PE_{eff}. Here we define PE_{eff} as POC export at 150m/time-integrated PP.

Uncertainties in the satellite-derived estimates of PP arise from the choice of algorithm applied to satellite Chl-*a* to estimate PP. Here we use the most widely-used algorithm (VGPM), which has also been shown to be among the best PP algorithms for the North Atlantic (Saba et al., 2011).

3. Results

3.1. ^{234}Th and ^{210}Po fluxes

^{234}Th and ^{210}Po fluxes (Tables S1, S2 and S3) were estimated using parent-daughter disequilibrium following equation 1.

During cruise D350 (Table S1), ^{234}Th fluxes were on average (± 1SD) 2168 ± 945 dpm m^{-2} d^{-1} at IRB and 1438 ± 197 dpm m^{-2} d^{-1} in the IB. During cruise D354 (Table S2 and S3), averaged ^{234}Th fluxes were: 2162 ± 995 dpm m^{-2} d^{-1} at IRB and 1520 ± 379 dpm m^{-2} d^{-1} in the IB, while ^{210}Po averaged 95 ± 24 dpm m^{-2} d^{-1} at IRB and 111 ± 23 dpm m^{-2} d^{-1} at IB. Additionally, a complete set of ^{234}Th, ^{210}Po and ^{210}Pb vertical profiles in depth for cruise D354 can be found in Figure S1 and S2.

One of the most remarkable results are the significant deficits (^{234}Th/^{238}U ratios < 0.90) found for several stations during D354 (namely stations 18, 20, 22, 24, 27, 28 and 33) between 400 and 500 m (Figure S2). Similar deficits at deep depths have been previously reported by other studies, such as Martin et al. (2011), Le Moigne et al. (2013) and Morris et al. (2007), who found disequilibria at 400 m in their studies of the Iceland Basin, the PAP Site and the Southern Ocean respectively. Furthermore, Pabortsava (2014) reported ^{234}Th deficits as deep as 1000 m in the Equatorial Atlantic. The reasons of these deep deficits remain unclear and need further investigations.

In the case of ^{210}Po/^{210}Pb profiles, secular equilibrium is not reached above 1000 m, except for station 27 (Figure S2). Below 1000 m stations 04, 16, 20 and 22 reported ^{210}Po/^{210}Pb ratios ranged between 0.4 and 0.6. Not many studies have measured ^{210}Po/^{210}Pb profiles below 1000 m and they

usually reported similar deficits at 1000 m, such as Le Moigne et al. (2013) at the PAP Site (ratios between 0.5 and 0.8), Rigaud et al. (2015) during the US GEOTRACES GA03 North Atlantic Section (ratios between 0.5 and 1), Hu et al. (2014) in the Aleutian Basin-Pacific Ocean (ratios between ~0.5 and 0.8) and Wei et al. (2014) in the SouthEast Asian Time-series Study (ratios between 0.6 and 0.8). On the other hand, Roca-Martí et al. (2016) and Rigaud et al. (2015) found secular equilibrium between ^{210}Po and ^{10}Pb below 1000 m in the Artic and over the North Atlantic continental shelf respectively.

The causes for the ^{210}Po deficits in deep waters have been extensively debated and several explanations have been proposed, although reasons remain unclear (Church et al., 2012; Rigaud et al., 2015).This disequilibrium might be associated with a ^{210}Po biochemical behaviour based on high adsorption combined with negligible desorption rates. However further investigations are needed to quantitatively define this last hypotheses.

3.2. Particulate organic matter to radionuclide ratios

The *POC:R* ratio was obtained from small (1-53 µm) and large (> 53 µm) particles collected using SAPS for both D350 and D354, and from sinking particles collected in the PELAGRA sediment trap (see section 2) for D354.

POC:R ratios measured using SAPS are shown in Tables S1, S2 and S3. During cruise D350 (Table S1), POC:Th ratios were on average (± 1SD) 11 ± 3 µmol dpm^{-1} at IRB and 15 ± 7 µmol dpm^{-1} in the IB for large particles; 5.9 ± 0.7 µmol dpm^{-1} at IRB and 4.5 ± 1.1 µmol dpm^{-1} at IB for small particles. During cruise D354 (Table S2 and S3), averaged POC:Th ratios for large particles were: 5.2 ± 1.7 µmol dpm^{-1} at IRB and 6.3 ± 1.4 µmol dpm^{-1} in the IB, while POC:Po averaged 99 ± 41 µmol dpm^{-1} at IRB and 114 ± 39 µmol dpm^{-1} at IB. For small particles POC:Th averaged 3.3 ± 0.7 µmol dpm^{-1} at IRB and 4.3 ± 1.8 µmol dpm^{-1} at IB and POC:Po averaged 92 ± 22 µmol dpm^{-1} at IRB and 113 ± 123 µmol dpm^{-1} at IB.

328 POC to radionuclide ratios measured by PELAGRAs are shown in Table 2. Averaged ratios for the
329 traps deployed at 150 m depth were: 7.7 ± 7.6 µmol dpm^{-1} at IRB and 6.0 ± 1.3 µmol dpm^{-1} at IB for
330 POC:Th; and 48 ± 15 µmol dpm^{-1} at IRB and 102 ± 49 µmol dpm^{-1} at IB for POC:Po.
331 All of the measured POC to radionuclide rations fall within the range of previously published
332 measurements. In the mid-Atlantic Ocean (Verdeny et al., 2009) ratios measured with pumps ranged
333 from 3.9 ± 0.5 µmol dpm^{-1} to 19.9 ± 1.3 µmol dpm^{-1} for POC:Th in particles > 53 µm, from 2.5 ± 0.3
334 µmol dpm^{-1} to 3.8 ± 0.3 µmol dpm^{-1} for POC:Th in particles > 0.7 µm, and from 1.4 ± 0.9 µmol
335 dpm^{-1} to 8.5 ± 6.9 µmol dpm^{-1} for POC:Po in particles > 0.7 µm. In the Sargasso Sea (EDDIE)
336 (Buesseler et al., 2008a) ratios ranged from 1.9 ± 0.8 µmol dpm^{-1} to 2.5 ± 0.3 µmol dpm^{-1} for
337 POC:Th, and from 25 µmol dpm^{-1} to 89 µmol dpm^{-1} for POC:Po in particles > 53 µm. In the
338 Mediterranean Sea (MedFlux) (Stewart et al., 2007) values ranged from 3.4 to 24.6 µmol dpm^{-1} for
339 POC:Th, and from 181 to 383 µmol dpm^{-1} for POC:Po in particles > 70 µm.

340 Regarding the ratios measured with traps, in the Sargasso Sea (EDDIE) (Buesseler et al., 2008a)
341 ranged from 1.7 ± 0.4 µmol dpm^{-1} to 4.1 ± 0.3 µmol dpm^{-1};and from 1.5 ± 0.2 µmol dpm^{-1} to 24.2 ±
342 9.1 µmol dpm^{-1} for POC:Th, and 23.5 ± 0.7 µmol dpm^{-1} to 373 ± 47 µmol dpm^{-1} for POC:Po in the
343 Mediterranean Sea (MedFlux) (Stewart et al., 2007).

344

345 *3.3. SAPS-derived carbon fluxes*

346 Two particle size classes were sampled by SAPS to determine the *POC:R* ratio. We estimate POC
347 export using only *POC:R* from >53 µm particles in order to allow comparison to other studies that
348 follow the same approach (Le Moigne et al., 2013b; Stewart et al., 2011), among many others, see
349 (Buesseler et al., 2006) for review on POC:Th ratios). Nonetheless, in section 4.1 we assess the
350 effect of the exclusion of small particles on the accuracy of our results.
351 During D350, the particle flux at MLD + 110 m for ^{234}Th- derived POC (Th-POC) averaged (± 1SD)
352 26 ± 15 mmol m^{-2} d^{-1} in the IRB and 21 ± 8 mmol m^{-2} d^{-1} in the IB (Table S1).

353 During D354, in the IRB, the particle flux at MLD + 110 m for Th-POC averaged 11 ± 7 mmol m^{-2} d^{-1}
354 and ranged between 5.0 ± 1.4 mmol m^{-2} d^{-1} (station 16) and 26 ± 13 mmol m^{-2} d^{-1} (station 24)
355 (Table S2). ^{210}Po-derived POC (Po-POC) fluxes were of a similar magnitude (on average 10 ± 4
356 mmol m^{-2} d^{-1} and ranged between 3.3 ± 0.6 mmol m^{-2} d^{-1} (station 08) and 15 ± 3 mmol m^{-2} d^{-1}
357 (station 20)) (Table S3). POC fluxes from both PELAGRA traps were much lower, ranging from 1.1
358 ± 0.1 to 1.6 ± 0.2 mmol m^{-2} d^{-1}, with an average value of 1.4 ± 0.1 mmol m^{-2} d^{-1} (Table 2).
359 In the IB, Th-POC fluxes were between 6.3 ± 2.1 mmol m^{-2} d^{-1} (station 06) and 12 ± 6 mmol m^{-2} d^{-1}
360 (station 27), and the average value was 9 ± 2 mmol m^{-2} d^{-1} (Table S2). Po-POC values ranged
361 between 5.5 ± 1.0 mmol m^{-2} d^{-1} (station 02) and 24 ± 4 mmol m^{-2} d^{-1} (station 33) and averaged 13 ±
362 6 mmol m^{-2} d^{-1} (Table S3). PELAGRA POC fluxes were 1.0 ± 0.1 and 2.7 ± 0.2 mmol m^{-2} d^{-1}
363 (Marsay et al., 2015) with a mean value of 1.9 ± 0.1 mmol m^{-2} d^{-1} (Table 2). In the following section
364 we first discuss the differences between PELAGRA and radionuclide-derived POC flux estimates
365 found in cruise D354 at MLD + 110 m. Secondly, we investigate potential reasons for the observed
366 discrepancies between methods, namely the contribution of slow sinking particles to POC export, the
367 use of instantaneous *POC:R* ratios for the ^{234}Th(^{210}Po) flux conversion into carbon fluxes and the
368 timescale covered by the methods. Finally, we combine our results with those obtained in other
369 studies that used PELAGRA and/or ^{234}Th and/or ^{210}Po to determine POC export, in order to
370 investigate how PE_{eff} changes with bloom phase.
371
372 **4. Discussion**
373 *4.1. Comparison of ^{234}Th- and ^{210}Po-derived POC fluxes to PELAGRA POC fluxes*
374 The base of the E_z -taken as the depth of 1% light penetration- extended between 42 and 47 m depth
375 during spring 2010 (cruise D350), and varied from 33 to 43 m depth during summer 2010 (cruise
376 D354) (Marsay, 2012). On the other hand, MLD was between 32 and 45 m during D341, and always
377 < 35 m during D354.

SAPS deployments were chosen at MLD + 10 m and MLD + 110 m (typically 50 and 150 m) following the same approach as Le Moigne et al. (2013b), while the shallower PELAGRA traps (typically at 80 m) were only successfully deployed on two occasions due to technical problems and storm damage (Marsay, 2012). In order to match all our objectives, MLD + 110 m (~150 m) was chosen as an integration depth.

Figure 2 shows the POC flux estimates calculated at MLD + 110 m (typically 150 m) using the three techniques in both IRB and IB. Attenuation of the POC flux is expected between the ~100 m of separation between the base of the E_z and the ~150 m sampling depth chosen. The choice of this integration depth was done because of the following reasons i) to have the same reference depth for the three PELAGRA, ^{234}Th and ^{210}Po POC derived fluxes; ii) to evaluate the carbon that penetrates into the mesopelagic zone, rather than the POC flux at the E_z.; and iii) to estimate the PE_{eff}, using the ratio PP to POC, that is usually defined at the 100-150 m depth (Buesseler, 1998; Henson et al., 2012).

^{234}Th and ^{210}Po deficits persist considerably below the E_z. Nevertheless, as long as ^{234}Th and ^{210}Po deficits still persist in the water column the radioactive pair techniques can be successfully applied.

According to Figure 2, there is no statistically significant difference between Th-POC and Po-POC fluxes in both regions (ANOVA test, $p = 0.11$ in the IB, and $p = 0.31$ in the IRB). However, PELAGRA-POC (Pe-POC) values are significantly different from both Th-POC and Po-POC fluxes (ANOVA test, $p = 0.05$ in the IB, and $p = 0.02$ in the IRB). Radionuclide-derived POC fluxes agree within uncertainties for most of the stations (as reported in previous studies, e.g. Le Moigne et al. (2013b), Stewart et al. (2011) and Wei et al. (2011)), with the exception of 5 specific stations: station 33 in the IB (Figure 2b); and stations 08, 15, 16 and 24 in the IRB (Figure 2c). Averaged Pe-POC values are one order of magnitude lower than averaged Th-POC and Po-POC in the two basins, in contradiction with previous studies that have reported good agreement between traps and radioanalytical techniques in both oligotrophic (e.g. Owens et al., (2013) at BATS using drifting trap

NBST and ^{234}Th; Stewart et al. (2011) also at BATS employing cylindrical traps, ^{234}Th and ^{210}Po; and Maiti et al. (2016) in the northern Gulf of Mexico sampling with surface-tethered drifting traps, ^{234}Th and ^{210}Po) and temperate regions (e.g. Le Moigne et al. (2013b) at the PAP Site using PELAGRA traps, ^{234}Th and ^{210}Po) . We will further analyse these discrepancies in section 4.2.

Large variations in ^{234}Th export fluxes were observed in the IRB (up to a factor of 2-3) during the spring cruise (D350, Table S1), while in the IB fluxes calculated at 4 stations were remarkably constant. The same feature is observed for the summer cruise (D354, Table S2). We consider that the differences between basins arise because the values correspond to very different regions in terms of both expanse and circulation and dynamics and the IRB is larger and more complex than the IB (Krauss, 1995). For ^{210}Po fluxes, only data during summer cruise are available and large variations are observed in both basins (Table S3). Note that that due to the combination of the currents flow and the half-life of both techniques, more especially for ^{210}Po, these results should not be ascribed to the specific station sampled, since the deficit collected might be originated elsewhere.

For this reason, we prefer not to refer our results to a particular station and we compare average results obtained within basins (Irminger/Iceland) or season (spring/summer). This is tightly related to the assumption of SS conditions that we address in section 4.2.1.

POC flux results are likely determined by two main factors: (1) the time scale associated with the method (Le Moigne et al., 2013b) and (2) the assumptions used to employ that method as a proxy for POC flux and PE_{eff}. We assume that PELAGRAs collect all the material sinking down, while for ^{234}Th and ^{210}Po, we normally consider that only large particles (>53 µm) contribute to the POC flux and assume SS conditions. These assumptions entail several implications that may alter the estimations of export presented in this study. In the following sections we assess the influence of these factors on PELAGRA-, Th- and Po-derived POC results, in order to investigate the differences in POC fluxes found in summer 2010.

4.1.1. *Contribution of small particles*

As previously explained, ^{234}Th and ^{210}Po fluxes are converted into carbon flux using the ratio *POC:R* in the settling particles. Traditionally, large particles are used to calculate *POC:R* as it was assumed that only large particles contributed significantly to the downward flux, with most of the small particles assumed to be remineralised in the euphotic zone (Bishop et al., 1977). However, recent studies have demonstrated that this assumption is not always valid (Alonso-González et al., 2010; Durkin et al., 2015; McDonnell and Buesseler, 2010; Riley et al., 2012; Villa-Alfageme et al., 2014). Therefore, to estimate the export, ideally *POC:R* from both large and small particles, and proportional to their contribution to the flux, should be used (Cavan et al., 2015; Le Moigne et al., 2013b). Therefore, equation 3 should be reformulated as

$$POC_{flux} = Th/Po_{flux} \cdot \left[\rho_{large} \cdot (POC:Th/Po)_{\substack{large \\ particles}} + \rho_{small} \cdot (POC:Th/Po)_{\substack{small \\ particles}} \right] \quad (4)$$

being ρ_{large} and ρ_{small} the contributions of both pools to the flux. In this case, unfortunately, we do not have information about relative flux contributions ($\rho_{large/small}$). For this reason, we can only qualitatively assess the influence of the unaccounted for small particles in the Th- and Po-POC derived flux estimates.

Figures 3a and 3b show POC:Th and POC:Po ratios in the small and large fractions of particles collected from SAPS. On one hand, Figure 3b shows that $(POC:Po)_{small}$ and $(POC:Po)_{large}$ ratios are very similar in most of the stations sampled (except for stations 28 and 33). Hence, Po-POC flux will not change significantly if there is contribution of small particles and $\rho_{small} \neq 0$, because POC:Po ratio is approximately constant. On the other hand $(POC:Th)_{small}$ and $(POC:Th)_{large}$ ratios are different for small and large sinking particles. Thus, if the contribution of small particles to the flux were significant, the Th-POC flux from Figure 2 would not be accurate, since we only consider that POC flux = Th flux $\cdot \rho_{large}(POC:Th)_{large\ particles}$. Furthermore, since $(POC:Th)_{large}$ ratios are systematically

451 higher than those in small particles for the vast majority of stations (Figure 3a), if there is a
452 contribution of small particles, the Th-POC fluxes presented here will be overestimated.
453 At MLD + 110 m, POC:Th ratios were found to be higher in large particles than in the small ones in
454 most of the stations, except for 15, 16, 27 and 28 -where ratios agreed within uncertainties- (Figure
455 3a and Table S5). At MLD + 10 m, ratios agreed within uncertainties for stations 08, 16 and 28 and
456 were found to be higher in small particles than in large for stations 06, 22 and 27 (Table S5). In the
457 remaining stations, ratios in large particles were found to be higher than in the small ones. On a basin
458 scale, POC:Th ratios in the IB and IRB were higher in large particles than in the small ones by 4%
459 and 26% respectively at MLD + 10 m and by 36% and 46% respectively at MLD + 110 m.
460 Higher POC:Th ratios with increasing particle size have been previously reported by several studies
461 (see review by Buesseler et al. (2006)) in contrast to the higher POC:Th ratios found in smaller
462 particles by Buesseler et al. (1995), Jacquet et al. (2011), Le Moigne et al. (2013b), Maiti et al.
463 (2016) and Puigcorbé et al. (2015). POC:Th ratios are significantly influenced by the structure of
464 plankton and particles composition, in some cases authors have claimed that greater POC:Th ratios
465 in small particles than in large particles are associated to a plankton community dominated by
466 smaller particles (Maiti et al., 2016; Puigcorbé et al., 2015). Unfortunately, we do not have the
467 required data of community structure to further investigate the reasons of the POC:Th ratios found.
468 To assess the amplitude of the potential overestimation, we consider two limit situations: (1) if POC
469 flux were equally divided between large and small particles, POC flux = Th flux · [0.5 ·
470 $(POC:Th)_{small\ particles}$ + 0.5 · $(POC:Th)_{large\ particles}$], according to equation 4, Th-POC fluxes would be
471 overestimated by 20% for both basins; (2) in the unlikely case of POC being exported exclusively by
472 small particles, the overestimation of Th-POC flux would be around 45%.
473 The overestimation is consistent with Verdeny et al. (2009) (several regions: Southern Ocean, South
474 and mid- Atlantic Ocean, Sargasso Sea, Mediterranean Sea and Equatorial Pacific) and Le Moigne et
475 al. (2013b) (PAP Site), which found that Th-POC fluxes were systematically higher than both Po-

476 POC and Pe-POC fluxes at 150 m. One of the potential explanations proposed by Le Moigne et al.
477 (2013b) was the non-inclusion of small particles, which in case it would result in an underestimation
478 of Po-POC fluxes (since in that region POC:Po were lower for the large size fraction than for the
479 small). When small particles contribute to export, this could partially explain the differences found
480 between Th- and Po-POC derived fluxes (Figure 2). However, the one order of magnitude
481 differences found between radionuclide-POC and Pe-POC estimates remain unexplained.
482
483 *4.1.2. Influence of variable ^{234}Th:POC and ^{210}Po:POC ratios*
484 In the IB, POC:Th ratios for large particles in the spring cruise increased significantly with depth
485 (~51%), while in the summer cruise they remained approximately constant (Tables S4 and S5). On
486 the contrary, in the IRB basin, POC:Th ratios decreased with depth by a similar amount (~30%)
487 (Table S4 and S5). POC:Po ratios decreased in both basins in the summer cruise (13% in the IB and
488 32% in the IRB), but no data from the spring cruise are available for comparison.
489 Figure 3a shows that POC:Th ratios for the large fraction of particles decreased in both basins
490 between the spring and summer cruises (D350 and D354 respectively). During this period there were
491 shifts in the zooplankton and phytoplankton community structures, most likely as a consequence of
492 changes in nutrient availability and mixing regimes. Cruise data suggests that coccolithophores were
493 a significant component of the phytoplankton community in the IB (Daniels et al., 2015; Poulton et
494 al., 2010), and in particular *Coccolithus pelagicus* were unusually dominant in the IRB during spring
495 (Henson et al., 2013).
496 Nonetheless, changes in community structure are not a determinant fact in the observed changes in
497 the *POC:R* ratios since two different species may play similar ecological functions and are not
498 necessarily responsible for the differences found between the two sites. Nonetheless, seasonal
499 changes in community structure are expected to generate variations in *POC:R* ratios through changes
500 in particle sinking velocity, particle shape, size, density, and aggregation rates, along with variations

in carbon assimilation rate by particles. It is difficult to specifically name and quantify the mechanisms involved; ultimately all the changes alter *POC:R* ratios (Buesseler et al., 2006) and many reasons propelled the clear shift in POC:Th ratios from spring to summer (Figure 3a).

Temporal changes in *POC:R* ratios might influence our estimates of radionuclide-derived POC fluxes by almost one order of magnitude (Figure 3a). If the *POC:R* ratio varies over time, there might be a discrepancy between the time scales covered by the ratio (which is approximately instantaneous on the day of sampling) and the ^{234}Th or ^{210}Po flux (which cover periods of weeks to months due to their half-lives), i.e. the ratios correspond to instantaneous measurements whereas Th and Po fluxes might be influenced by past events. Hence, measured ratios might not be fully representative of the ratios of sinking particles that created the measured flux. The maximum uncertainty induced by this can potentially be assessed by the change in the POC:Th ratios between the spring and summer cruises: on average 36% in the IRB and 41% in the IB.

4.2. Influence of time scale on POC flux estimates and the steady state approach

The distribution of ^{234}Th and ^{210}Po activities in the water column is mainly controlled by radioactive decay, scavenging rate by particulate material and by physical processes. The sinking of particles carrying ^{234}Th and ^{210}Po creates a deficit of these radionuclides relative to their parents, ^{238}U and ^{210}Pb respectively. Theoretically, half of this deficit persists for at least 1 and 3 months respectively in the water column as a consequence of ^{234}Th and ^{210}Po half-lives (24.1 d and 138.4 d). This implies that the vertical distribution of ^{234}Th and ^{210}Po in the water column reflects processes of particle dynamics that occurred on a time scale of several weeks (^{234}Th) to months (^{210}Po) before sampling. On the other hand, PELAGRA traps directly catch the sinking material while they are deployed (~ 50 hours). This means that PELAGRAs only record recent export events. Therefore, the export flux calculated by the three techniques will depend on the past and/or present phase of the bloom and the

three methods will only agree if a period of low temporal variability in export is sampled (Le Moigne et al., 2013b).

During cruise D354, biogeochemical conditions were atypical. Satellite-derived Chl-*a* in the IRB typically depicts a short, intense bloom in spring, followed by a summer minimum (Henson et al., 2006). For the region of the IB, the typical annual phytoplankton bloom starts in early April and peaks in late June (Achterberg et al., 2013). However, satellite-derived bloom timing indicated a later bloom in the Central IRB than elsewhere in the IB and the Western IRB in summer 2010 (Ryan-Keogh et al., 2013). Figures 4a and 4b show that in the IRB, the bloom started in early May (western basin: DOY ~135), but instead of rapidly reaching a peak in spring before dying out in summer, Chl-*a* concentration continued to rise, finally peaking in mid-July (central basin: DOY 192, 1.9 mg Chl-*a* m^{-3}). These Chl-*a* concentrations were anomalously high (2-3 times higher than typical for this region) and elevated concentrations persisted through autumn 2010 (Henson et al., 2013). In the IB, satellite-derived Chl-*a* seems to indicate a peak from early April through to late May. During July, both regions usually present post-bloom conditions (Nielsdóttir et al., 2009; Sanders et al., 2005; Waniek and Holliday, 2006). However in 2010 the bloom was unexpectedly long and persisted into the summer, especially in the Central IRB (Henson et al., 2013; Ryan-Keogh et al., 2013).

Our hypothesis is that the approximately order of magnitude difference between POC fluxes reported by PELAGRA and the radioanalytical techniques is because the three methods account for export occurring over very different timeframes and portions of the bloom period.

We believe that the decisive factor is that PELAGRAS and ^{234}Th and ^{210}Po deficits are associated to different events of export and carbon flux. When PELAGRA were released (between DOY 194 and 216) there was a peak in the PP (around DOY 195, Figure 4b), yet the export in the mesopelagic was low, likely as a result of high remineralization rates due to higher temperatures than in spring and strong zooplankton reworking and repackaging (Marsay et al., 2015; Villa-Alfageme et al., 2016). This resulted in a relatively low POC fluxes recorded by PELAGRAS.

On the contrary, the higher POC fluxes reported by both ^{234}Th and ^{210}Po suggest that both techniques recorded a previous event of higher export when PP was also high (~1500 mmol m^{-2} d^{-1}).

To support this hypothesis, we present Th-POC results from cruise D350, which sampled the area ~70 days before cruise D354 (see section 2.1). Th-POC averaged values of 26 ± 15 mmol m^{-2} d^{-1} in the IRB and 21 ± 8 mmol m^{-2} d^{-1} in the IB, Table S1) confirm a previous high export in both basins. ^{234}Th results shows that the spring POC export flux is more than twice as large as than the Th-POC measured in summer in both basins, despite the fact that PP peak was reached in DOY ~195. Similar high POC flux values in the first stages of the spring bloom have also been reported at the PAP Site by (Villa-Alfageme et al., 2016), who measured Po-POC averaged values of 25 ± 7 mmol m^{-2} d^{-1} in 2012 as part of cruise JC071 (see section 2.1 and Table 1 for more details).

This suggests that events of high export happen in the first stages of blooms and POC export in spring can be maximum, despite the relatively low PP. This way, export events during the persisting spring/summer bloom of 2010 (Henson et al., 2013; Ryan-Keogh et al., 2013) created a large and long lasting deficit of ^{234}Th and ^{210}Po that had not fully decayed by the time of sampling (Figures S1 and S2) and resulted in the high Th- and Po-POC fluxes measured. Thus, despite the fact that in mid-July PP reached its peak and started declining, the ^{234}Th and ^{210}Po deficits were still representative of high export associated with the earlier bloom (Figure 4a and 4b).

Note that ^{234}Th and ^{210}Po cover different time scales backwards due to the different half-lives; their deficits persist in water, governed by their half-lives. The similar POC results reported by both ^{234}Th and ^{210}Po techniques suggest that the timeframe covered by both radionuclides overlapped. According to Equation 1, deficits do not accumulate over time so we do not expect Po-POC fluxes higher than Th-POC fluxes (Le Moigne et al., 2013b; Stewart et al., 2011; Verdeny et al., 2009). Therefore, Th-POC and Po-POC fluxes coincide when the station is sampled shortly after the export event that creates both deficits. Th-POC and Po-POC would report different POC fluxes if, for instance, the station is sampled after the ^{234}Th deficit decayed but the ^{210}Po deficit still persists, i.e.

575 respectively more than one month and less than three months after the export event started and
576 ended. This will depend on the kind of bloom, the sampling moment, and the bloom progress since
577 the beginning of the export to the sampling moment. In our sampling cruise, the events recorded by
578 ^{234}Th-^{238}U and ^{210}Po-^{210}Pb deficit took place within the timeframe of both techniques. This means
579 more than ~30 days for ^{234}Th, and ~200 days for ^{210}Po, with the ^{210}Po timeframe presumably limited
580 by the lack of ^{210}Pb-^{210}Po disequilibrium before the bloom started (see section 4.3 for more details).
581
582 *4.2.1. Steady state approach assessment.*
583 Steady state conditions are generally assumed when using ^{234}Th and ^{210}Po techniques as a proxy for
584 POC flux (Bacon et al., 1976; Buesseler et al., 1998, 2001; Le Moigne et al., 2013b; Nozaki and
585 Tsunogai, 1976; Owens et al., 2015; Stewart et al., 2011, 2010; Thomalla et al., 2006). Under this
586 assumption, it is considered that ^{234}Th and ^{210}Po activities remain invariant over time, i.e. an
587 equilibrium between the nuclear decay of parent and daughter radionuclides and the removal of ^{234}Th
588 and ^{210}Po by particles has been reached. Since both ^{234}Th and ^{210}Po disequilibrium persist in the
589 water column according to their half-lives, the SS assumption provides an estimation of the real flux
590 of the moment only when the export is in a relatively long lasting plateau. On the contrary, in
591 situations of high export variability, the persistence of the deficits over time results in an estimation
592 of the real flux delayed in time proportionally to the radionuclide half-life when applying the SS
593 approach.
594 Situations of stable export occur when production, sinking of carbon and attenuation reach an
595 equilibrium. Such conditions are expected in well-established post-bloom conditions, and also likely
596 along the bloom for blooms with a gradual progression of the production.
597 POC export in the mesopelagic was evaluated using PELAGRA, ^{234}Th and ^{210}Po methods in post-
598 bloom condition at the PAP Site during summer 2009 by Le Moigne et al. (2013b). The bloom
599 associated with this cruise was significantly different to the bloom in the IRB and IB (Figure 4c and

4d). Stations were occupied during cruise D341 (Table 1) between DOY 194 and 220, several weeks after the Chl-*a* and PP started to decline after the spring peak (DOY ~160; Figure 4c and 4d). Averaged POC flux estimates integrated at MLD+ 110 m, and only considering large particles, were: 7.9 ± 4.7 mmol m^{-2} d^{-1} for Th-POC, 3.2 ± 1.6 mmol m^{-2} d^{-1} for Po-POC, and 2.3 ± 1.8 mmol m^{-2} d^{-1} for Pe-POC (Le Moigne et al., 2013b). In contrast to our IRB/IB 2010 results, estimates of export flux from the three techniques agree within uncertainties. We believe that this is because conditions were in a well-developed post-bloom state and therefore, export was in a plateau situation. Chl-*a* and PP time series (Figure 4c and 4d) show that, at the PAP site, the time gap between the decline of the bloom and the start of sampling (~ 34 d, Figures 4c and 4d) is sufficiently long to allow both ^{234}Th and ^{210}Po deficits to decay. In conclusion, at the PAP Site, PELAGRA, ^{234}Th and ^{210}Po were all recording the same export event -the declining phase of the bloom- and the SS approach was proved to be valid to predict the real export flux at the sampling moment in a post-bloom situation.

Similarly, in oligotrophic regions -approximately in steady state conditions (Maiti et al., 2016)- export results in a persisting plateau even during bloom periods and the three techniques record the same export events. Therefore, good agreement between trap-derived, ^{234}Th-derived and ^{210}Po-derived POC fluxes is usually found, as reported by several studies (e.g. Maiti et al. (2016), Owens et al. (2013) and Stewart et al. (2011)).

Radionuclide techniques are able to detect increments in export by means of increments in their deficits but instantaneous reductions in the export might be masked by a previous, relatively recent, persisting deficits.

In contrast with PAP site, in our summer sampling (D354) there is an export variability as a consequence of the bloom progression. Therefore, when we applied the radionuclide techniques to the present time, the low export at time of the sampling (accurately recorded by PELAGRAs) was masked by the larger deficits generated by a higher previous export. As a result, both ^{234}Th and ^{210}Po techniques misreported the present declining phase of the export and, on the contrary, reported

higher POC values that corresponded to a previous phase of the bloom. In conclusion, under situations of high export variability, the SS approach is not valid to predict the real export flux at the sampling moment, but provides an accurate delayed estimation of the POC export previous to the sampling. The bloom progress and the stage of bloom must be analysed in relation to the sampling moment to correctly identify the export event associated with the radionuclide-derived export estimates.

4.3. Effect of seasonal variability on PE_{eff} estimates

In this section we compare the PE_{eff} obtained using PELAGRA, ^{234}Th and ^{210}Po-derived fluxes and discuss implications for interpretation of PE_{eff}.

To estimate PP, we integrate satellite-derived PP over the period of time represented by the technique (see methods). For the PELAGRA export efficiency (PeE_i) estimation, Pe-POC flux is associated with the PP averaged over the 8 days previous to the PELAGRA recovery along the path of the PELAGRA trajectories, assuming that traps travelled in a straight line and at constant speed between deployment and recovery. For Th- and Po-derived export efficiencies (ThE_i and PoE_i respectively), Th-POC and Po-POC fluxes are associated with the PP averaged over the period that Th/U and Po/Pb deficits persist in the water column (i.e. 30 days for ThE_i and 90 days for PoE_i). In calculating integrated PP, the pre-bloom period should be excluded, because the radionuclide deficit only starts to develop when significant biological activity and export occur, i.e. with the start of the spring bloom.

Note that, due to the long ^{210}Po half-life and the deepening of the MLD during winter, ^{210}Po-^{210}Pb deficit might persists during the winter and previous to the bloom. This initial deficit is usually unaccounted for and would result in an overestimation of both ^{210}Po and Po-POC flux. Nonetheless, the good agreement between Th-POC and Po-POC in our case of study suggests that this deficit is negligible.

650 Thus, for PoE_i, PP must be integrated only from the time when the bloom started to the time of
651 sampling in order to not underestimate PoE_i estimates. The start of the bloom was determined
652 according to the criteria proposed by Siegel et al. (2002) (i.e. date on which the Chl-*a* concentration
653 exceeded a threshold value more than 5% of the annual median) and was calculated as DOY 121 in
654 IB and DOY 145 in IRB (Figure 4a). In the case of our cruise D354, this means ~3 months and
655 therefore, 90 days were chosen for PP integration.
656 Table 3 shows averaged PE_{eff} values obtained by this approach during cruise D354 in the HLNA.
657 Averaged estimates (with 1SD) are: i) 0.7 ± 0.3% for PeE_i, 9 ± 4% for ThE_i and 11 ± 5% for PoE_i in
658 the IRB; and ii) 1.1 ± 0.6% for PeE_i, 6.2± 1.5% for ThE_i and 11 ± 5% for PoE_i in the IB. On a basin
659 scale, PeE_i is approximately one order of magnitude lower than ThE_i and PoE_i, while the
660 radionuclide techniques agree within uncertainties.
661 Average PP for the two basins over eight days, one month and three months prior to sampling is 183,
662 139 and 108 mmol m^{-2} d^{-1} respectively. Despite being significantly different (ANOVA test, $p < 0.01$), these differences in PP are an order of magnitude smaller than the discrepancies in PE_{eff}.
663
664 Hence, discrepancies in PE_{eff} are expected to be driven by the differences in the POC flux, as a
665 consequence of the method used and the bloom conditions, rather than PP.
666 This is confirmed by the analysis of the PE_{eff} in the three additional cruises that employed at least one
667 of the three techniques compared in this study (Table 1): those occupied in spring/early summer
668 (D350 in the HLNA, and JC071 in the PAP Site; see section 2.1) and the one occupied in summer at
669 the PAP site (D341, see section 2.1). Chl-*a* concentration and PP time series for these cruises are
670 shown in Figures 4a-4b, 4e-4f and 4c-4d respectively.
671 Figure 5 compiles all the PE_{eff} estimates, as a function of the sampling time, location and technique
672 employed (summary in Table 1). Average ThE_i values for IRB and IB in spring (D350) are 52 ± 39%
673 and 50 ± 18% respectively, which are significantly higher than the ThE_i measured in summer
674 (D354), 9 ± 2 % and 6.2 ± 1.6% respectively. Similarly PoE_i decreases from 55 ± 13% at the PAP

site in spring (JC071), to 2.7 ± 1.4% in mid-July (D341). These results show that both at the PAP site and in the HLNA, there is a pronounced decrease in PE_{eff} from the formation of the bloom (early spring) to the late stages of the bloom (Figure 5). Average values for PE_{eff} estimated with the two other techniques during the D341 are: 2.1 ± 1.6% for PeE_i and 5.6 ± 3.3% for ThE_i. As previously stated (section 4.2.1), the post-bloom period was sample in this cruise. In this scenario, the results do not differ significantly within techniques, likely because they sampled the same export event, i.e. the declining bloom, and therefore POC fluxes (and PE_{eff}) are similar. Furthermore, PE_{eff} in this post-bloom stage of the bloom were very similar at both PAP site (~4%) and the IRM the IB (~7%). Which suggest that the low export flux detected by PELAGRA at the IRB and IB is not an isolated case

Therefore, results of Figure 5 suggest that export efficiency varies along the bloom and it decreases as the bloom progress. We propose that the observed decline in PE_{eff} from spring to summer is probably due to evolution of the surface plankton community structure and changes in the hydrographic conditions (mainly temperature, (Marsay et al., 2015; Yvon-Durocher et al., 2012)) in the upper mesopelagic during the bloom, which affect the export efficiency. High export efficiencies at the beginning of the bloom would be associated to lower remineralization and higher aggregation rates, while lower export efficiencies, and lower POC export would be associated to higher remineralization (due to higher temperatures) (Marsay et al., 2015) and repackaging and reworking by zooplankton (Villa-Alfageme et al., 2016).

Martin et al. (2011) found that the spring diatom bloom in the HLNA was associated with fast-sinking diatom aggregates that contained transparent exopolymer particles. Additionally, it is often assumed that in highly seasonal high latitude regions, zooplankton grazing (and packaging function) is not able to keep pace with phytoplankton growth during the initial stages of the bloom (Lam et al., 2011). Surface remineralisation rates, likely dependent on temperature as shown in Marsay et al.

699 (2015), would be lower in spring than in summer. As a result, particles would be exported very
700 efficiently in the early phases of the bloom.
701 A decrease in PE_{eff} in post-bloom conditions is likely associated with higher surface particle
702 recycling rates. Higher water temperatures may lead to higher metabolic rates of particle attached
703 bacteria and thus higher remineralisation. Piontek et al. (2015) showed that changes in the type of
704 dissolved organic matter may counteract the increase of remineralisation rates by the increase of
705 temperature. This may be also valid for particles but, unfortunately, it is not possible to test here. In
706 addition, strong zooplankton grazing control of phytoplankton biomass is typical of developed
707 blooms (Calbet, 2001; Calbet and Landry, 2004). Furthermore, sinking particles at MLD + 110 m in
708 late summer were found to be smaller and slower settling (Villa-Alfageme et al., 2016), making them
709 more prone to be consumed by bacteria and zooplankton.
710 Our conclusions have important implications for using *in situ* measurements to derive algorithms to
711 estimate the annual and/or global carbon exported. Such estimates generally assume that the
712 instantaneous PE_{eff} estimate is representative of the annual mean and can thus be applied to annual
713 total PP to obtain annual total export (Henson et al., 2011; Laws et al., 2000). Therefore, when
714 compiling data from multiple different studies to derive global-scale PE_{eff} algorithms using large
715 databases (Le Moigne et al., 2013a), particular attention should be paid to the methods used
716 (specifically their inherent timescales) and the phase of the bloom at the time of sampling.
717

718 **5. Summary and conclusions**

719 POC fluxes using three different techniques, PELAGRA traps, ^{234}Th and ^{210}Po, estimated during
720 summer 2010 in two regions of the HLNA (IB and IRB) revealed discrepancies of over one order of
721 magnitude. Neither the contribution of small particles, nor the variations in POC:Th and POC:Po
722 ratios accounted for the differences in the POC flux estimates. The seasonal variability of PE_{eff} was

analysed through the comparison of PELAGRA, and/or ^{234}Th, and/or ^{210}Po-derived fluxes in two locations from the temperate North Atlantic and in different bloom phases.

Our key findings are:

1. Differences between PELAGRA, ^{234}Th and ^{210}Po techniques in estimating POC fluxes are due to a combination of the different time scales covered by the techniques and the stage of the bloom at the time of sampling. Therefore we recommend to characterise the bloom phase (e.g. through study of satellite-derived PP time series), to correctly interpret the information provided by the techniques.
2. The steady-state assumption approach provides an estimation of the real flux of the moment only when the export is in a relatively long lasting plateau. In situations of high export variability, it results in an estimation of the real flux delayed in time proportionally to the radionuclide half-life and the bloom progress and the stage of bloom must be analysed in relation to the sampling moment in order to correctly identify the export event associated to the radionuclide-derived export estimates.
3. PELAGRA, ^{234}Th and ^{210}Po are expected to provide similar values of PE_{eff} if the three methods are used in a clear post-bloom situation and presumably at the start of a bloom or a long time after it, when the system is temporally invariant. Conversely, PE_{eff} estimates from different methods will differ strongly when sampling occurs during a period of rapid change in export, e.g. during the declining phase of the bloom. In this case, PELAGRA-derived estimates of PE_{eff} will be lower than Th- or Po-derived estimates.
4. Comparison of the three techniques suggest a strong seasonal variability in PE_{eff} in the North Atlantic. Export efficiency is greatest in the first stages of the bloom and declines as the season progresses (from ~ 50% in spring to ~ 3% in summer). Formation of aggregates, lower remineralisation rates and reduced zooplankton grazing are all equally valid reasons for higher export efficiency at the beginning of the bloom.

5. When compiling *in situ* data for the purposes of developing algorithms to estimate annual export flux, we must ensure that individual POC flux or PE_{eff} estimates are comparable. For that, we have to take into account the phase of the bloom and the technique used

Acknowledgments

We thank the captain and crew of the RRS Discovery during research cruises D350 and D354, alongside the chief scientists (C.M. Moore, E. Achterberg) and all the scientists involved in both cruises for help, support and advice. The Ocean Productivity website (http://www.science.oregonstate.edu/ocean.productivity/) is acknowledged for providing primary production data. This work was supported by the Natural Environment Research Council (NERC, UK) through the Irminger basin Iron study (IBIS) project NE/E006833/1, (E.P.A. and C.M.M.), the European Union, CalMarO, 215157, R.J.S., F.A.C.L.M), Obra Social "la Caixa" (Spain) through a Grant for Graduate Studies (E.C.R.) and V Research Plan from Universidad de Sevilla (M.V.A.). FACLM is now supported the Cluster of Excellence 80 'The Future Ocean' (grant: CP1403) Initiative by the Deutsche Forschungsgemeinschaft (DFG).

Tables

Table 1. Sampling site and dates for the four cruises considered, and number of stations sampled for each of the three techniques and for SAPS deployments (with measurements made on SAPS samples).

Location	Dates	Cruise number	^{234}Th	^{210}Po	PELAGRA	SAPS
Irminger Basin (IRB)	Spring 2010 26/04-09/05 sampled in IRB	D350	4 stations	0 stations	0 stations	4 stations POC, ^{234}Th
Irminger Basin (IRB)	Summer 2010 04/07-11/08 sampled in IRB	D354	8 stations	8 stations	2 stations	8 stations POC, ^{234}Th, ^{210}Po, ^{210}Pb
Iceland Basin (IB)	Spring 2010 26/04-09/05 sampled in IB	D350	3 stations	0 stations	0 stations	3 stations POC, ^{234}Th
Iceland Basin (IB)	Summer 2010 04/07-11/08 sampled in IB	D354	7 stations	7 stations	2 stations	7 stations POC, ^{234}Th, ^{210}Po, ^{210}Pb
Porcupine Abyssal Plain (PAP)	Summer 2009 13/07-08/08 sampled in PAP	D341	10 stations	9 stations	3 stations	10 stations POC, ^{234}Th, ^{210}Po, ^{210}Pb
Porcupine Abyssal Plain (PAP)	Spring 2012 01/05-08/05 sampled in PAP	JC071	0 stations	4 stations	0 stations	4 stations POC, ^{210}Po, ^{210}Pb

Table 2. PELAGRA trap numbers, sampling start and ending date and time details, depths and sampling durations during cruise D354 and measured POC fluxes, POC:Th and POC:Po ratios (propagated uncertainties are also indicated).

PELAGRA trap numbers	Deployment depth (m)	Sampling start date/time	Sampling end date/time	Sampling duration (h)	POC flux (mmol m^{-2} d^{-1})	POC:Th (μmol dpm^{-1})	POC:Po (μmol dpm^{-1})
P6-1	156 ± 5	13/07/10 01:00	14/07/10 07:22	30	1.02 ± 0.06	5.0 ± 0.5	67 ± 8

P6-2	152 ± 6	19/07/10 01:30	21/07/10 08:54	54	1.14 ± 0.05	13 ± 1	58 ± 8
P4-3	84 ± 5	26/07/10 08:00	28/07/10 04:00	44	2.0510	5.4 ± 0.4	51 ± 5
P6-3	154 ± 4	26/07/10 08:30	28/07/10 10:54	50	1.56 ± 0.08	2.3 ± 0.2	37 ± 5
P7-3	402 ± 4	26/07/10 07:30	28/07/10 03:30	44	0.45 ± 0.05	2.4 ± 0.2	25 ± 3
P4-4	82 ± 5	04/08/10 008:30	06/08/10 00:30	404	4.36 ± 0.19	10 ± 1	120 ± 13
P6-4	152 ± 5	04/08/10 09:00	06/08/10 07:23	46	2.66 ± 0.15	6.9 ± 0.6	136 ± 24
P7-4	402 ± 6	04/08/10 08:00	06/08/10 00:00	40	1.37 ± 0.07	5.1 ± 0.5	54 ± 7

Table 3. PELAGRA-, Th- and Po- derived particle export efficiency (PeE_i, ThE_i, PoE_i) in % (uncertainties and standard deviation of the spatial average are also indicated) for D354, the associated PP and the resulting averaged PE_{eff} (standard deviation of the spatial average is also indicated). Stations without results for some of the variables are denoted by nan.

	PELAGRA	PP 8 days average (mmol $m^{-2}d^{-1}$)	PeE_i %	Station	PP 30 days average (mmol $m^{-2}d^{-1}$)	ThE_i %	PP 90 days average (mmol $m^{-2}d^{-1}$)	PoE_i %
IB	P6-1	153.4	0.7 ± 0.1	02	126.8	nan	96.3	5.7 ± 3.1
	P6-4	176.6	1.5 ± 0.1	04	147.4	6.7 ± 2.9	120.2	8.0 ± 2.1
				06	146.0	4.3 ± 1.4	115.4	8.4 ± 4.0
				27	148.8	8.3 ± 4.1	128.1	11 ± 6
				28	138.2	6.5 ± 2.4	133.7	11 ± 3
				31	203.9	nan	146.1	9.5 ± 2.1
				33	153.0	5.3 ± 2.2	113.6	21 ± 6
average			1.1 ± 0.6			6.2 ± 1.5		11 ± 5
IRB	P6-2	230.2	0.5 ± 0.1	08	125.5	10 ± 1	83,6	3.9 ± 1.7
	P6-3	176.0	0.9 ± 0.1	10	91.1	11 ± 4	68,1	9.4 ± 3.2
				15	133.1	4.3 ± 1.3	92,1	13 ± 4
				16	105.4	4.6 ± 1.3	85,5	14 ± 7

				18	169.1	7.5 ± 1.4	119,5	11 ± 5
				20	103.4	13 ± 3.7	79,9	19 ± 8
				22	111.5	6.0 ± 2.2	104,2	4.9 ± 2.2
				24	163.5	16 ± 8	127.4	9.0 ± 3.2
average			0.7 ± 0.3			9 ± 4		11 ± 5

References

Achterberg, E.P.C., Moore, M., Henson, S.A., Steigenberger, S., Stohl, A., Eckhardt, S., Avendano, L.C., Cassidy, M., Hembury, D., Klar, J.K., Lucas, M.I., Macey, A.I., Marsay, C.M., Ryan-Keogh, T.J., 2013. Natural iron fertilization by the Eyjafjallajökull volcanic eruption. Geophys. Res. Lett. 40, 921–926–921–926.

Alonso-González, I.J., Arístegui, J., Lee, C., Sanchez-Vidal, A., Calafat, A., Fabrés, J., Sangrá, P., Masqué, P., Hernández-Guerra, A., Benítez-Barrios, V., 2010. Role of slowly settling particles in the ocean carbon cycle. Geophys. Res. Lett. 37, n/a-n/a. doi:10.1029/2010GL043827

Antia, A.N., Koeve, W., Gerhard, F., Thomas, B., Detlef, S.-B., Jan, S., Susanne, N., Klaus, K., Joachim, K., Rolf, P., Dirk, H., Ulrich, B., Maureen, C., Uwe, F., B., Z., 2001. Basin-wide particulate carbon flux in the Atlantic Ocean: Regional export patterns and potential for atmospheric CO2 sequestration. Global Biogeochem. Cycles 15.

Bacon, M.P., Spencer, D.W., Brewer, P.G., 1976. 210Pb/226Ra and 210Po/210Pb disequilibria in seawater and suspended particulate matter. Earth Planet. Sci. Lett. 32, 277–296. doi:http://dx.doi.org/10.1016/0012-821X(76)90068-6

Banse, K., 1990. New views on the degradation and disposition of organic particles as collected by sediment traps in the open sea. Deep Sea Res. Part A. Oceanogr. Res. Pap. 37, 1177–1195. doi:http://dx.doi.org/10.1016/0198-0149(90)90058-4

Baskaran, M., Church, T., Hong, G., Kumar, A., Qiang, M., Choi, H., Rigaud, S., Maiti, K., 2013. Effects of flow rates and composition of the filter, and decay/ingrowth correction factors involved with the determination of in situ particulate ^{210}Po and ^{210}Pb in seawater. Limnol. Oceanogr. Methods 11, 126–138. doi:10.4319/lom.2013.11.126

Behrenfeld, M.J., Falkowski, P.G., 1997. Photosynthetic rates derived from satellite-based chlorophyll concentration. Limnol. Oceanogr. 42, 1–20. doi:10.4319/lo.1997.42.1.0001

Bishop, J.K.B., Edmond, J.M., Ketten, D.R., Bacon, M.P., Silker, W.B., 1977. The chemistry, biology, and vertical flux of particulate matter from the upper 400 m of the equatorial Atlantic Ocean. Deep Sea Res. 24, 511–548. doi:http://dx.doi.org/10.1016/0146-6291(77)90526-4

Bishop, J.K.B., Lam, P.J., Wood, T.J., 2012. Getting good particles: Accurate sampling of particles by large volume in-situ filtration. Limnol. Oceanogr. Methods 10, 681–710. doi:10.4319/lom.2012.10.681

Buesseler, K., Ball, L., Andrews, J., Benitez-Nelson, C., Belastock, R., Chai, F., Chao, Y., 1998. Upper ocean export of particulate organic carbon in the Arabian Sea derived from thorium-234. Deep Sea Res. Part II Top. Stud. Oceanogr. 45, 2461–2487. doi:http://dx.doi.org/10.1016/S0967-0645(98)80022-2

Buesseler, K.O., 1998. The decoupling of production and particulate export in the surface ocean. Global Biogeochem. Cycles 12, 297–310. doi:10.1029/97GB03366

Buesseler, K.O., Andrews, J.A., Hartman, M.C., Belastock, R., Chai, F., 1995. Regional estimates of the export flux of particulate organic carbon derived from thorium-234 during the JGOFS EqPac program. Deep Sea Res. Part II Top. Stud. Oceanogr. 42, 777–804. doi:http://dx.doi.org/10.1016/0967-0645(95)00043-P

Buesseler, K.O., Benitez-Nelson, C., van der Loeff, M.R., Andrews, J., Ball, L., Crossin, G., Charette, M.A., 2001. An intercomparison of small- and large-volume techniques for thorium-234 in seawater. Mar. Chem. 74, 15–28.

Buesseler, K.O., Benitez-Nelson, C.R., Moran, S.B., Burd, A., Charette, M., Cochran, J.K., Coppola, L., Fisher, N.S., Fowler, S.W., Gardner, W.D., Guo, L.D., Gustafsson, Ö., Lamborg, C., Masque, P., Miquel, J.C., Passow, U., Santschi, P.H., Savoye, N., Stewart, G., Trull, T., 2006. An assessment of particulate organic carbon to thorium-234 ratios in the ocean and their impact on the application of 234Th as a POC flux proxy. Mar. Chem. 100, 213–233.

Buesseler, K.O., Lamborg, C., Cai, P., Escoube, R., Johnson, R., Pike, S., Masque, P., McGillicuddy, D., Verdeny, E., 2008a. Particle fluxes associated with mesoscale eddies in the Sargasso Sea. Deep Sea Res. Part II Top. Stud. Oceanogr. 55, 1426–1444.

Buesseler, K.O., Trull, T.W., Steinberg, D.K., Silver, M.W., Siegel, D.A., Saitoh, S.I., Lamborg, C.H., Lam, P.J., Karl, D.M., Jiao, N.Z., Honda, M.C., Elskens, M., Dehairs, F., Brown, S.L., Boyd, P.W., Bishop, J.K.B., Bidigare, R.R., 2008b. VERTIGO (VERtical Transport In the Global Ocean): A study of particle sources and flux attenuation in the North Pacific. Deep Sea Res. Part II Top. Stud. Oceanogr. 55, 1522–1539. doi:http://dx.doi.org/10.1016/j.dsr2.2008.04.024

Calbet, A., 2001. Mesozooplankton grazing effect on primary production: A global comparative analysis in marine ecosystems. Limnol. Oceanogr. 46, 1824–1830. doi:10.4319/lo.2001.46.7.1824

Calbet, A., Landry, M.R., 2004. Phytoplankton growth, microzooplankton grazing, and carbon cycling in marine systems. Limnol. Oceanogr. 49, 51–57. doi:10.4319/lo.2004.49.1.0051

Cavan, E.L., Le Moigne, F.A.C., Poulton, A.J., Tarling, G.A., Ward, P., Daniels, C.J., Fragoso, G.M., Sanders, R.J., 2015. Attenuation of particulate organic carbon flux in the Scotia Sea, Southern Ocean, is controlled by zooplankton fecal pellets. Geophys. Res. Lett. 42, 2014GL062744. doi:10.1002/2014GL062744

Chen, J.H., Edwards, R.L., Wasserburg, G.J., 1986. 238U,234U and232Th in seawater. Earth Planet. Sci. Lett. 80, 241–251.

Church, T., Rigaud, S., Baskaran, M., Kumar, A., Friedrich, J., Masque, P., Puigcorbé, V., Kim, G., Radakovitch, O., Hong, G., Choi, H., Stewart, G., 2012. Intercalibration studies of ^{210}Po and ^{210}Pb in dissolved and particulate seawater samples. Limnol. Oceanogr. Methods 10, 776–789. doi:10.4319/lom.2012.10.776

Cochran, J.K., Buesseler, K.O., Bacon, M.P., Livingston, H.D., 1993. Thorium isotopes as indicators of particle dynamics in the upper ocean: results from the JGOFS North Atlantic Bloom experiment. Deep Sea Res. Part I Oceanogr. Res. Pap. 40, 1569–1595.

Daniels, C.J., Poulton, A.J., Esposito, M., Paulsen, M.L., Bellerby, R., St John, M., Martin, A.P., 2015. Phytoplankton dynamics in contrasting early stage North Atlantic spring blooms: composition, succession, and potential drivers. Biogeosciences 12, 2395–2409. doi:10.5194/bg-12-2395-2015

De La Rocha, C.L., Passow, U., 2007. Factors influencing the sinking of POC and the efficiency of the biological carbon pump. Deep Sea Res. Part II Top. Stud. Oceanogr. 54, 639–658. doi:http://dx.doi.org/10.1016/j.dsr2.2007.01.004

Ducklow, H.W., Kirchman, D.L., Anderson, T.R., 2002. The magnitude of spring bacterial production in the North Atlantic Ocean. Limnol. Ocean. 47, 1684–1693.

Durkin, C.A., Estapa, M.L., Buesseler, K.O., 2015. Observations of carbon export by small sinking particles in the upper mesopelagic. Mar. Chem. 175, 72–81. doi:http://dx.doi.org/10.1016/j.marchem.2015.02.011

Giering, S.L.C., Sanders, R., Lampitt, R.S., Anderson, T.R., Tamburini, C., Boutrif, M., Zubkov, M. V, Marsay, C.M., Henson, S.A., Saw, K., Cook, K., Mayor, D.J., 2014. Reconciliation of the carbon budget in the ocean/'s twilight zone. Nature 507, 480–483. doi:10.1038/nature13123

Gómez-Guzmán, J.M., Villa, M., Le Moigne, F., López-Gutiérrez, J.M., García-León, M., 2013. AMS measurements of 129I in seawater around Iceland and the Irminger Sea. Nucl. Instruments Methods Phys. Res. Sect. B Beam Interact. with Mater. Atoms 294, 547–551. doi:http://dx.doi.org/10.1016/j.nimb.2012.07.045

Henson, S.A., Dunne, J.P., Sarmiento, J.L., 2009. Decadal variability in North Atlantic phytoplankton blooms. J. Geophys. Res. Ocean. 114, C04013. doi:10.1029/2008JC005139

Henson, S.A., Painter, S.C., Penny Holliday, N., Stinchcombe, M.C., Giering, S.L.C., 2013. Unusual subpolar North Atlantic phytoplankton bloom in 2010: Volcanic fertilization or North Atlantic

Oscillation? J. Geophys. Res. Ocean. 118, 4771–4780. doi:10.1002/jgrc.20363
Henson, S.A., R., S., E., M., J., M.P., L., M.F., Quartly, G.D., 2011. A reduced estimate of the strength of the ocean's biological carbon pump. Geophys. Res. Lett. 38.
Henson, S.A., Richard, S., Claire, H., Allen, J.T., 2006. Timing of nutrient depletion, diatom dominance and a lower-boundary estimate of export production for Irminger Basin, North Atlantic. Mar. Ecol. Prog. Ser. 313, 73–84. doi:10.3354/meps313073
Henson, S.A., Sanders, R., Madsen, E., 2012. Global patterns in efficiency of particulate organic carbon export and transfer to the deep ocean. Global Biogeochem. Cycles 26, n/a-n/a.
Henson, S.A., Yool, A., Sanders, R., 2015. Variability in efficiency of particulate organic carbon export: A model study. Glob. Biogeochem. Cycles 29, 33–45.
Hu, W., Chen, M., Yang, W., Zhang, R., Qiu, Y., Zheng, M., 2014. Enhanced particle scavenging in deep water of the Aleutian Basin revealed by ^{210}Po-^{210}Pb disequilibria. J. Geophys. Res. Ocean. 119, 3235–3248. doi:10.1002/2014JC009819
Jacquet, S.H.M., Lam, P.J., Trull, T., Dehairs, F., 2011. Carbon export production in the subantarctic zone and polar front zone south of Tasmania. Deep Sea Res. Part II Top. Stud. Oceanogr. 58, 2277–2292. doi:http://dx.doi.org/10.1016/j.dsr2.2011.05.035
Krauss, W., 1995. Currents and mixing in the Irminger Sea and in the Iceland Basin. J. Geophys. Res. 100, 10851. doi:10.1029/95JC00423
Kwon, E.Y., Primeau, F., L., S.J., 2009. The impact of remineralization depth on the air-sea carbon balance. Nat. Geosci 2, 630–635.
Lam, P.J., Doney, S.C., Bishop, J.K.B., 2011. The dynamic ocean biological pump: Insights from a global compilation of particulate organic carbon, CaCO3, and opal concentration profiles from the mesopelagic. Global Biogeochem. Cycles 25, n/a-n/a. doi:10.1029/2010GB003868
Lamborg, C.H., Buesseler, K.O., Valdes, J., Bertrand, C.H., Bidigare, R., Manganini, S., Pike, S., Steinberg, D., Trull, T., Wilson, S., 2008. The flux of bio- and lithogenic material associated with sinking particles in the mesopelagic "twilight zone" of the northwest and North Central Pacific Ocean. Deep Sea Res. Part II Top. Stud. Oceanogr. 55, 1540–1563. doi:http://dx.doi.org/10.1016/j.dsr2.2008.04.011
Lampitt, R.S., Bett, B.J., Kiriakoulakis, K., Popova, E.E., Ragueneau, O., Vangriesheim, A., Wolff, G.A., 2001. Material supply to the abyssal seafloor in the Northeast Atlantic. Prog. Oceanogr. 50, 27–63. doi:http://dx.doi.org/10.1016/S0079-6611(01)00047-7
Lampitt, R.S., Boorman, B., Brown, L., Lucas, M., Salter, I., Sanders, R., Saw, K., Seeyave, S., Thomalla, S.J., Turnewitsch, R., 2008. Particle export from the euphotic zone: Estimates using a novel drifting sediment trap, 234Th and new production. Deep Sea Res. Part I Oceanogr. Res. Pap. 55, 1484–1502.
Laws, E.A., Falkowski, P.G., Smith, W.O., Ducklow, H., McCarthy, J.J., 2000. Temperature effects on export production in the open ocean. Global Biogeochem. Cycles 14, 1231–1246. doi:10.1029/1999GB001229
Le Moigne, F.A.C., Henson, S.A., Cavan, E., Georges, C., Pabortsava, K., Achterberg, E.P., Ceballos-Romero, E., Zubkov, M., Sanders, R.J., 2016. What causes the inverse relationship between primary production and export efficiency in the Southern Ocean? Geophys. Res. Lett. n/a-n/a. doi:10.1002/2016GL068480
Le Moigne, F.A.C., Henson, S.A., Sanders, R.J., Madsen, E., 2013a. Global database of surface ocean particulate organic carbon export fluxes diagnosed from the 234Th technique. Earth Syst. Sci. Data 5, 295–304.
Le Moigne, F.A.C., Moore, C.M., Sanders, R.J., Villa-Alfageme, M., Steigenberger, S., Achterberg, E.P., 2014a. Sequestration efficiency in the iron limited North Atlantic: Implications for iron supply mode to fertilized blooms. Geophys. Res. Lett.
Le Moigne, F.A.C., Pabortsava, K., Marcinko, C.L.J., Martin, P., Sanders, R.J., 2014b. Where is mineral ballast important for surface export of particulate organic carbon in the ocean?

Geophys. Res. Lett. 41, 2014GL061678. doi:10.1002/2014GL061678
Le Moigne, F.A.C., Poulton, A.J., Henson, S.A., Daniels, C.J., Fragoso, G.M., Mitchell, E., Richier, S., Russell, B.C., Smith, H.E.K., Tarling, G.. A., Young, J.R., Zubkov, M., 2015. Carbon export efficiency and phytoplankton community composition in the Atlantic sector of the Arctic Ocean. J. Geophys. Res. Ocean. 120, 3896–3912. doi:10.1002/2015JC010700
Le Moigne, F.A.C., Villa-Alfageme, M., Sanders, R.J., Marsay, C., Henson, S., García-Tenorio, R., 2013b. Export of organic carbon and biominerals derived from 234Th and 210Po at the Porcupine Abyssal Plain. Deep Sea Res. Part I Oceanogr. Res. Pap. 72, 88–101.
Maiti, K., Bosu, S., D'Sa, E.J., Adhikari, P.L., Sutor, M., Longnecker, K., 2016. Export fluxes in northern Gulf of Mexico - Comparative evaluation of direct, indirect and satellite-based estimates. Mar. Chem. 184, 60–77. doi:10.1016/j.marchem.2016.06.001
Maiti, K., Buesseler, K.O., Pike, S.M., Benitez-Nelson, C., Cai, P., Chen, W., Cochran, K., Dai, M., Dehairs, F., Gasser, B., Kelly, R.P., Masque, P., Miller, L.A., Miquel, J.C., Moran, S.B., Morris, P.J., Peine, F., Planchon, F., Renfro, A.A., van der Loeff, M.R., Santschi, P.H., Turnewitsch, R., Waples, J.T., Xu, C., 2012. Intercalibration studies of short-lived thorium-234 in the water column and marine particles. Limnol. Oceanogr. Methods 10, 631–644. doi:10.4319/lom.2012.10.631
Marsay, C.M., 2012. Particulate Trace Metals, Carbon and Nitrogen in the Mesopelagic (phdthesis).
Marsay, C.M., Sanders, R.J., Henson, S.A., Pabortsava, K., Achterberg, E.P., Lampitt, R.S., 2015. Attenuation of sinking particulate organic carbon flux through the mesopelagic ocean. Proc. Natl. Acad. Sci. 112, 1089–1094.
Martin, P., Lampitt, R.S., Perry, M.J., Sanders, R., Lee, C., D'Asaro, E., 2011. Export and mesopelagic particle flux during a North Atlantic spring diatom bloom. Deep Sea Res. Part I Oceanogr. Res. Pap. 58, 338–349.
McDonnell, A.M.P., Buesseler, K.O., 2010. Variability in the average sinking velocity of marine particles. Limnol. Oceanogr. 55, 2085–2096. doi:10.4319/lo.2010.55.5.2085
Morris, P.J., Sanders, R., Robert, T., Sandy, T., 2007. 234Th-derived particulate organic carbon export from an island-induced phytoplankton bloom in the Southern Ocean. Deep. Res. Part II 54, 2208–2232.
Nielsdóttir, M.C., Moore, C.M., Sanders, R., Hinz, D.J., Achterberg, E.P., 2009. Iron limitation of the postbloom phytoplankton communities in the Iceland Basin. Glob. Biogeochem. Cycles 23.
Nozaki, Y., Tsunogai, S., 1976. 226Ra, 210Pb and 210Po disequilibria in the Western North Pacific. Earth Planet. Sci. Lett. 32, 313–321. doi:http://dx.doi.org/10.1016/0012-821X(76)90071-6
Owens, S.A., Buesseler, K.O., Lamborg, C.H., Valdes, J., Lomas, M.W., Johnson, R.J., Steinberg, D.K., Siegel, D.A., 2013. A new time series of particle export from neutrally buoyant sediments traps at the Bermuda Atlantic Time-series Study site. Deep Sea Res. Part I Oceanogr. Res. Pap. 72, 34–47. doi:http://dx.doi.org/10.1016/j.dsr.2012.10.011
Owens, S.A., Pike, S., Buesseler, K.O., 2015. Thorium-234 as a tracer of particle dynamics and upper ocean export in the Atlantic Ocean. Deep Sea Res. Part II Top. Stud. Oceanogr. 116, 42–59. doi:http://dx.doi.org/10.1016/j.dsr2.2014.11.010
Pabortsava, K., 2014. Downward Particle Export and Sequestration Fluxes in the Oligotrophic Atlantic Ocean. University of Southampton.
Painter, S.C., Lucas, M.I., Stinchcombe, M.C., Bibby, T.S., Poulton, A.J., 2010. Summertime trends in pelagic biogeochemistry at the Porcupine Abyssal Plain study site in the northeast Atlantic. Deep Sea Res. Part II Top. Stud. Oceanogr. 57, 1313–1323. doi:http://dx.doi.org/10.1016/j.dsr2.2010.01.008
Parekh, P., Dutkiewicz, S., Follows, M.J., Ito, T., 2006. Atmospheric carbon dioxide in a less dusty world. Geophys. Res. Lett. 33. doi:10.1029/2005GL025098
Peterson, M.L., Fabres, J., Wakeham, S.G., Lee, C., Alonso, I.J., Miquel, J.C., 2009. Sampling the vertical particle flux in the upper water column using a large diameter free-drifting NetTrap

adapted to an Indented Rotating Sphere sediment trap. Deep Sea Res. Part II Top. Stud. Oceanogr. 56, 1547–1557. doi:http://dx.doi.org/10.1016/j.dsr2.2008.12.020

Pike, S.M., Buesseler, K.O., Andrews, J., Savoye, N., 2005. Quantification of 234Th recovery in small volume sea water samples by inductively coupled plasma-mass spectrometry. J. Radioanal. Nucl. Chem. 263, 355–360.

Piontek, J., Sperling, M., Nöthig, E.-M., Engel, A., 2015. Multiple environmental changes induce interactive effects on bacterial degradation activity in the Arctic Ocean. Limnol. Oceanogr. 60, 1392–1410. doi:10.1002/lno.10112

Poulton, A.J., Charalampopoulou, A., Young, J.R., Tarran, G.A., Lucas, M.I., Quartlya, G.D., 2010. Coccolithophore dynamics in non-bloom conditions during late summer in the central Iceland Basin (July-August 2007). Limnol. Oceanogr. 55, 1601–1613. doi:10.4319/lo.2010.55.4.1601

Poulton, A.J., Sanders, R., Holligan, P.M., Stinchcombe, M.C., Adey, T.R., Brown, L., Chamberlain, K., 2006. Phytoplankton mineralization in the tropical and subtropical Atlantic Ocean. Global Biogeochem. Cycles 20, GB4002. doi:10.1029/2006GB002712

Puigcorbé, V., Benitez-Nelson, C.R., Masqué, P., Verdeny, E., White, A.E., Popp, B.N., Prahl, F.G., Lam, P.J., 2015. Small phytoplankton drive high summertime carbon and nutrient export in the Gulf of California and Eastern Tropical North Pacific. Global Biogeochem. Cycles 29, 2015GB005134. doi:10.1002/2015GB005134

Rigaud, S., Stewart, G., Baskaran, M., Marsan, D., Church, T., 2015. 210Po and 210Pb distribution, dissolved-particulate exchange rates, and particulate export along the North Atlantic US GEOTRACES GA03 section. Deep. Res. Part II 116, 60–78. doi:10.1016/j.dsr2.2014.11.003

Riley, J.S., Sanders, R., Marsay, C., Moigne, F.A.C. Le, Achterberg, E.P., Poulton, A.J., 2012. The relative contribution of fast and slow sinking particles to ocean carbon export. Glob. Biogeochem. Cycles 26 (GB1026.

Roca-Martí, M., Puigcorbé, V., Rutgers van der Loeff, M.M., Katlein, C., Fernández-Méndez, M., Peeken, I., Masqué, P., 2016. Carbon export fluxes and export efficiency in the central Arctic during the record sea-ice minimum in 2012: a joint ^{234}Th/^{238}U and ^{210}Po/^{210}Pb study. J. Geophys. Res. Ocean. 121, 5030–5049. doi:10.1002/2016JC011816

Rutgers Van Der Loeff, M.M., Friedrich, J., Bathmann, U. V, 1997. Carbon export during the Spring Bloom at the Antarctic Polar Front, determined with the natural tracer 234Th. Deep Sea Res. Part II Top. Stud. Oceanogr. 44, 457–478. doi:http://dx.doi.org/10.1016/S0967-0645(96)00067-7

Ryan-Keogh, T.J., Macey, A.I., Nielsdóttir, M.C., Lucas, M.I., Steigenberger, S.S., Stinchcombe, M.C., Achterberg, E.P., Bibby, T.S., Moore, C.M., 2013. Spatial and temporal development of phytoplankton iron stress in relation to bloom dynamics in the high-latitude North Atlantic Ocean. Limnol. Oceanogr. 58, 533–545. doi:10.4319/lo.2013.58.2.0533

Saba, V.S., Friedrichs, M.A.M., Antoine, D., Armstrong, R.A., Asanuma, I., Behrenfeld, M.J., Ciotti, A.M., Dowell, M., Hoepffner, N., Hyde, K.J.W., Ishizaka, J., Kameda, T., Marra, J., Mélin, F., Morel, A., O 'reilly, J., Scardi, M., Smith, W.O., Smyth, T.J., 2011. An evaluation of ocean color model estimates of marine primary productivity in coastal and pelagic regions across the globe. Biogeosciences 8, 489–503. doi:10.5194/bg-8-489-2011

Salter, I., Lampitt, R.S., Sanders, R., Poulton, A., Kemp, A.E.S., Boorman, B., Saw, K., Pearce, R., 2007. Estimating carbon, silica and diatom export from a naturally fertilised phytoplankton bloom in the Southern Ocean using PELAGRA: A novel drifting sediment trap. Deep Sea Res. Part II Top. Stud. Oceanogr. 54, 2233–2259. doi:http://dx.doi.org/10.1016/j.dsr2.2007.06.008

Sanders, R., Brown, L., Henson, S., Lucas, M., 2005. New production in the Irminger Basin during 2002. J. Mar. Syst. 55, 291–310.

Sanders, R., Henson, S.A., Koski, M., Rocha, C.L.D. La, Painter, S.C., Poulton, A.J., Riley, J., Salihoglu, B., Visser, A., Yool, A., Bellerby, R., Martin, A., 2014. The Biological Carbon Pump in the North Atlantic. Prog. Oceanogr.

Sarmiento, J.L., Toggweiler, J.R., 1984. A new model for the role of the oceans in determining atmospheric PCO2. Nature 308, 621–624.
Savoye, N., Benitez-Nelson, C., Burd, A.B., Cochran, J.K., Charette, M., Buesseler, K.O., Jackson, G.A., Roy-Barman, M., Schmidt, S., Elskens, M., 2006. 234Th sorption and export models in the water column: A review. Mar. Chem. 100, 234–249.
Siegel, D.A., Buesseler, K.O., Doney, S.C., Sailley, S.F., Behrenfeld, M.J., Boyd, P.W., 2014. Global assessment of ocean carbon export by combining satellite observations and food-web models. Glob. Biogeochem. Cycles 28, 181–196–181–196.
Siegel, D.A., Doney, S.C., Yoder, J.A., 2002. The North Atlantic Spring Phytoplankton Bloom and Sverdrup's Critical Depth Hypothesis. Science (80-.). 296, 730–733.
Stewart, G., Cochran, J.K., Miquel, J.C., Masqué, P., Szlosek, J., Rodriguez y Baena, A.M., Fowler, S.W., Gasser, B., Hirschberg, D.J., 2007. Comparing POC export from 234Th/238U and 210Po/210Pb disequilibria with estimates from sediment traps in the northwest Mediterranean. Deep Sea Res. Part I Oceanogr. Res. Pap. 54, 1549–1570. doi:10.1016/j.dsr.2007.06.005
Stewart, G., Moran, S.B., Lomas, M.W., Kelly, R.P., 2011. Direct comparison of 210Po, 234Th and POC particle-size distributions and export fluxes at the Bermuda Atlantic Time-series Study (BATS) site. J. Environ. Radioact. 102, 479–489.
Stewart, G.M., Moran, S.B., Lomas, M.W., 2010. Seasonal POC fluxes at BATS estimated from 210Po deficits. Deep Sea Res. Part I Oceanogr. Res. Pap. 57, 113–124.
Thomalla, S., Turnewitsch, R., Lucas, M., Poulton, A., 2006. Particulate organic carbon export from the North and South Atlantic gyres: The 234Th/238U disequilibrium approach. Deep Sea Res. Part II Top. Stud. Oceanogr. 53, 1629–1648.
Valdes, J.R., Price, J.F., 2000. A Neutrally Buoyant, Upper Ocean Sediment Trap. J. Atmos. Ocean. Technol. 17, 62–68. doi:10.1175/1520-0426(2000)017<0062:ANBUOS>2.0.CO;2
van der Loeff, M.M., Geibert, W., 2008. Chapter 7 U- and Th-Series Nuclides as Tracers of Particle Dynamics, Scavenging and Biogeochemical Cycles in the Oceans, in: Radioactivity in the Environment. pp. 227–268. doi:10.1016/S1569-4860(07)00007-1
Verdeny, E., Masqué, P., Garcia-Orellana, J., Hanfland, C., Cochran, J.K., Stewart, G.M., 2009. POC export from ocean surface waters by means of 234Th/238U and 210Po/210Pb disequilibria: A review of the use of two radiotracer pairs. Deep Sea Res. Part II Top. Stud. Oceanogr. 56, 1502–1518.
Villa-Alfageme, M., de Soto, F., Le Moigne, F.A.C., Giering, S.L.C., Sanders, R., García-Tenorio, R., 2014. Observations and modeling of slow-sinking particles in the twilight zone. Global Biogeochem. Cycles 28, 2014GB004981. doi:10.1002/2014GB004981
Villa-Alfageme, M., de Soto, F.C., Ceballos, E., Giering, S.L.C., Le Moigne, F.A.C., Henson, S., Mas, J.L., Sanders, R.J., 2016. Geographical, seasonal, and depth variation in sinking particle speeds in the North Atlantic. Geophys. Res. Lett. doi:10.1002/2016GL069233
Volk, T., Hoffert, M.I., 1985. Ocean carbon pumps: Analysis of relative strengths and efficiencies in ocean-driven atmospheric CO2 changes. American Geophysical Union, pp. 99–110. doi:10.1029/GM032p0099
Waniek, J.J., Holliday, N.P., 2006. Large-scale physical controls on phytoplankton growth in the Irminger Sea, Part II: Model study of the physical and meteorological preconditioning. J. Mar. Syst. 59, 219–237.
Wei, C.-L., Lin, S.-Y., Sheu, D.D.-D., Chou, W.-C., Yi, M.-C., Santschi, P.H., Wen, L.-S., 2011. Po) as tracers for the estimation of export production in the South China Sea. Biogeosciences 8, 3793–3808. doi:10.5194/bg-8-3793-2011
Wei, C.-L., Yi, M.-C., Lin, S.-Y., Wen, L.-S., Lee, W.-H., 2014. Po in the northern South China Sea. Biogeosciences 11, 6813–6826. doi:10.5194/bg-11-6813-2014
Yvon-Durocher, G., Caffrey, J.M., Cescatti, A., Dossena, M., Giorgio, P. del, Gasol, J.M., Montoya, J.M., Pumpanen, J., Staehr, P.A., Trimmer, M., Woodward, G., Allen, A.P., 2012. Reconciling

the temperature dependence of respiration across timescales and ecosystem types. Nature 487, 472–476. doi:10.1038/nature11205

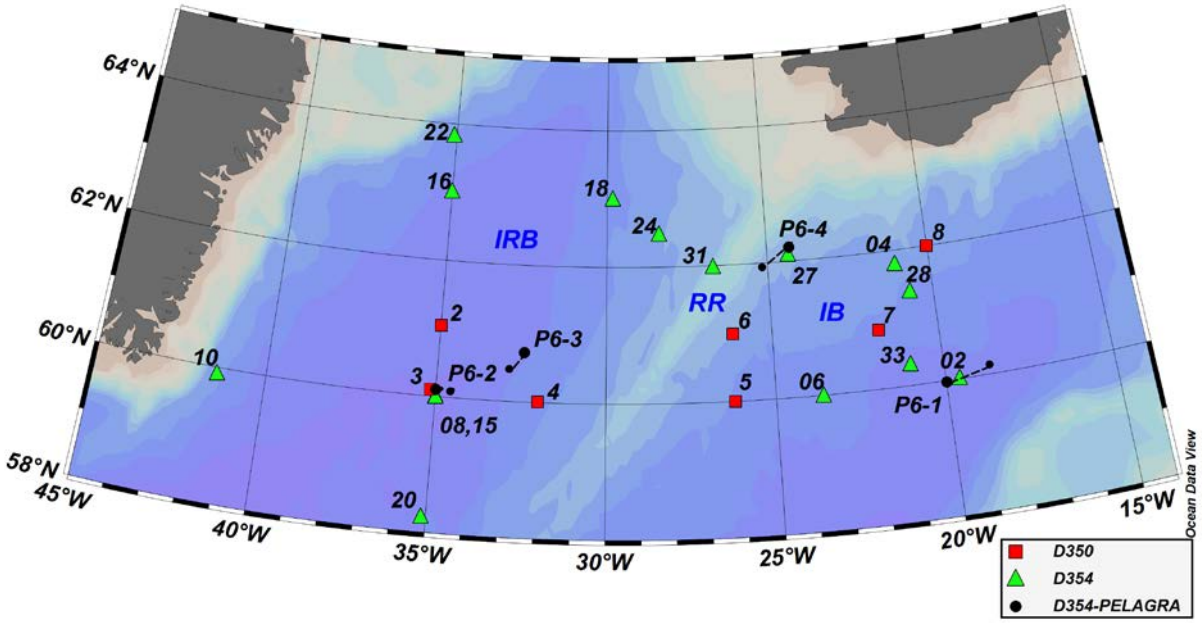

Figure 1. Map of the sampling area for cruises D350 and D354 in the Irminger Basin (IRB) and Iceland Basin (IB) and the Reykjanes Ridge (RR). PELAGRA deployment locations during D354 (large black dots) and the first recorded locations of the traps upon resurfacing (small black dots) are also included. Deployment and resurfacing locations are linked by a dashed line. Note that only traps used in the discussion were plotted (i.e. PELAGRA deployed at MLD + 110 m (typically 150m): P6-i, where P6 is trap ID number and i = deployment number {1, 4}).

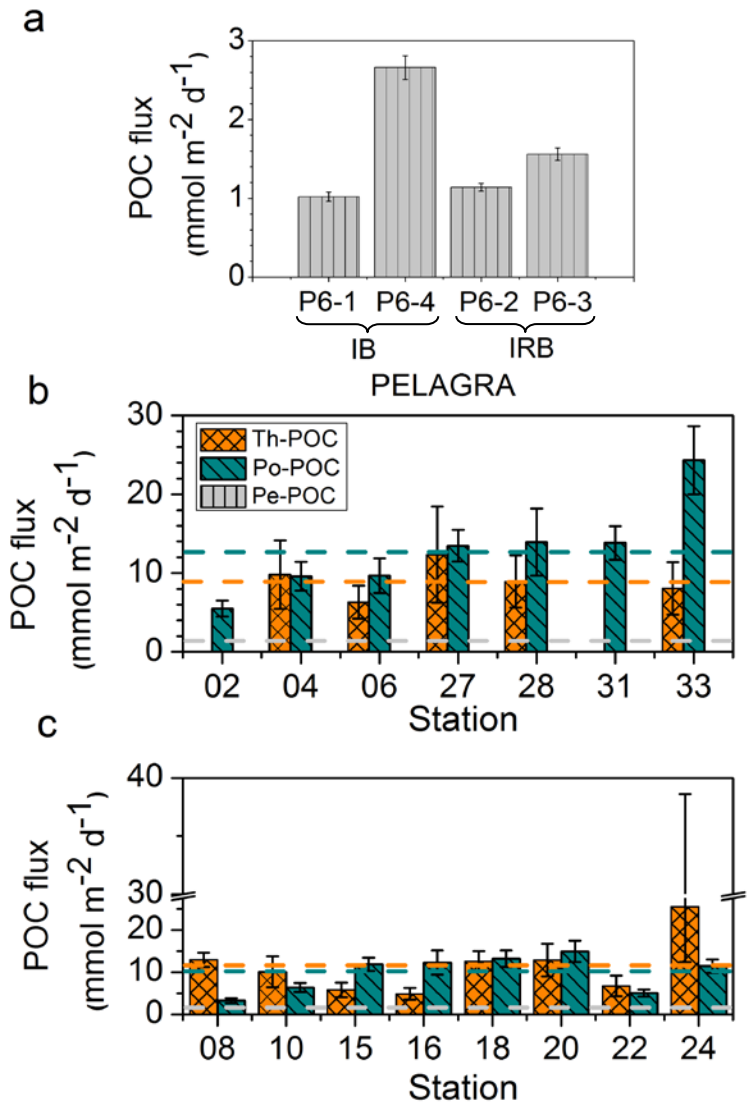

Figure 2. (a) PELAGRA-derived (Pe-POC) fluxes for the four trap deployments; and ^{234}Th-, ^{210}Po-derived POC fluxes in both (b) IB and (c) IRB at MLD + 110m (typically 150 m). The error bars indicate the propagated uncertainty. The horizontal dashed lines show the average value of the POC flux in the region for the three methods.

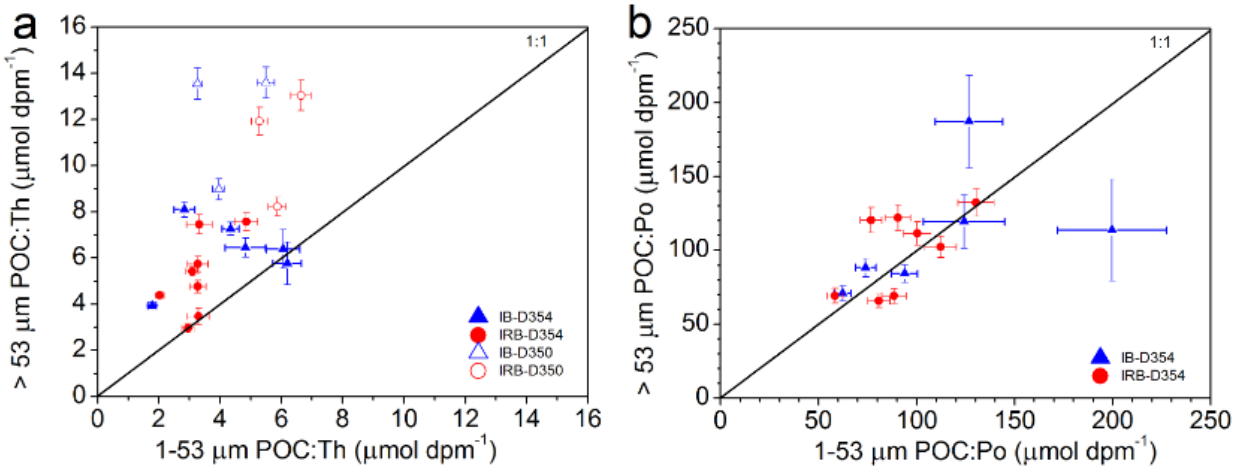

Figure 3. POC:radionuclide ratios (µmol dpm^{-1}) in > 53 µm versus 1-53 µm size-fractions measured in particles collected by SAPS at MLD + 110 m (typically 150 m) are shown for (a) Th; and (b) Po distinguished by basin. The 1:1 line is indicated in the figure.

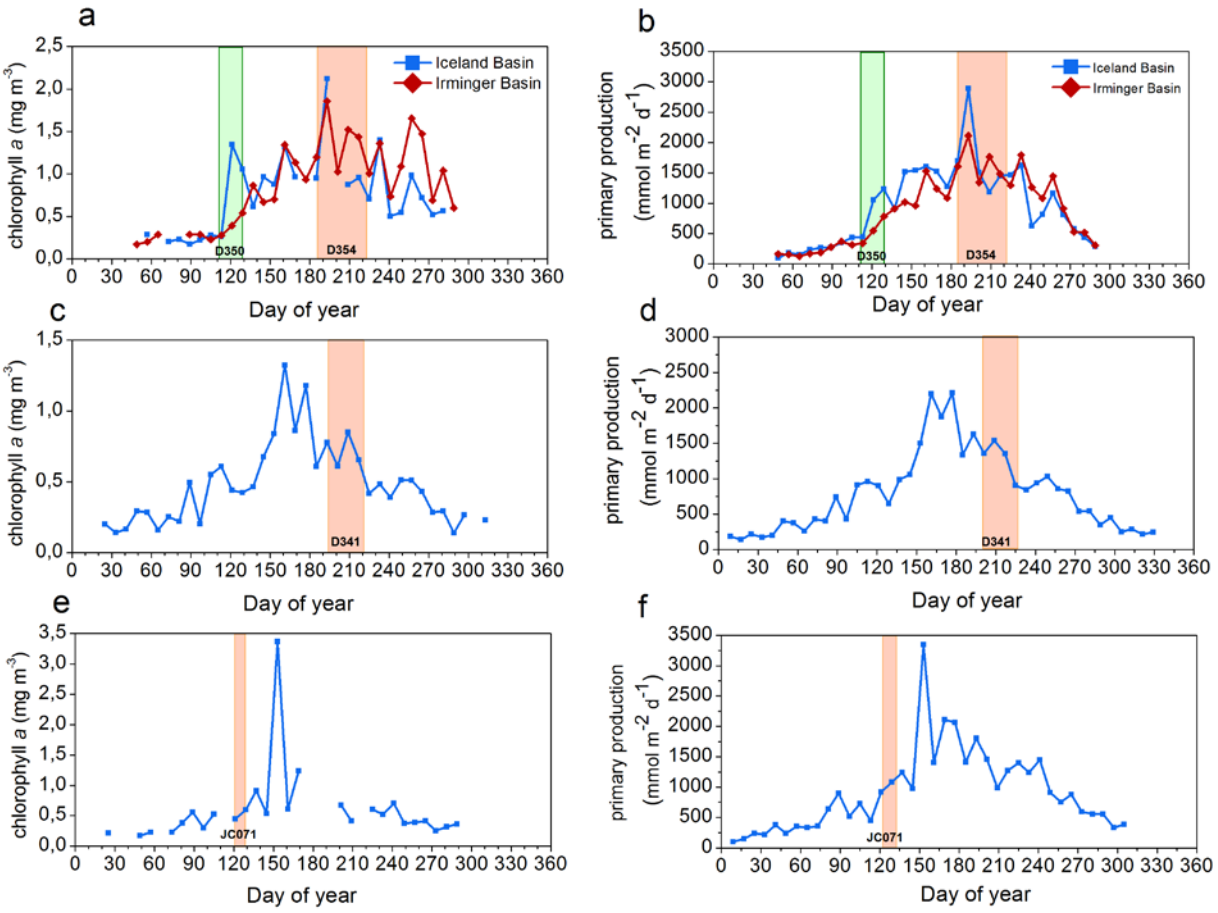

Figure 4. (a) MODIS satellite-derived chlorophyll *a* concentrations and (b) primary production (calculated using the VGPM algorithm (Behrenfeld and Falkowski, 1997)) derived from MODIS satellite-derived

chlorophyll *a* concentrations for 2010 in the IRB and IB. The timing of cruises D350 and D354 are shown by the green and orange shaded areas between days 116-129, and 185-223 respectively (Marsay *et al.*, 2015). Also shown are corresponding plots (c) and (d) for the Porcupine Abyssal Plain site in 2009, with the timing of cruise D341 shown by the shaded area between days 194 – 220; and plots (e) and (f) for the Porcupine Abyssal Plain in 2012, with the timing of cruise JC071 shown by the shaded area between days 122-129.

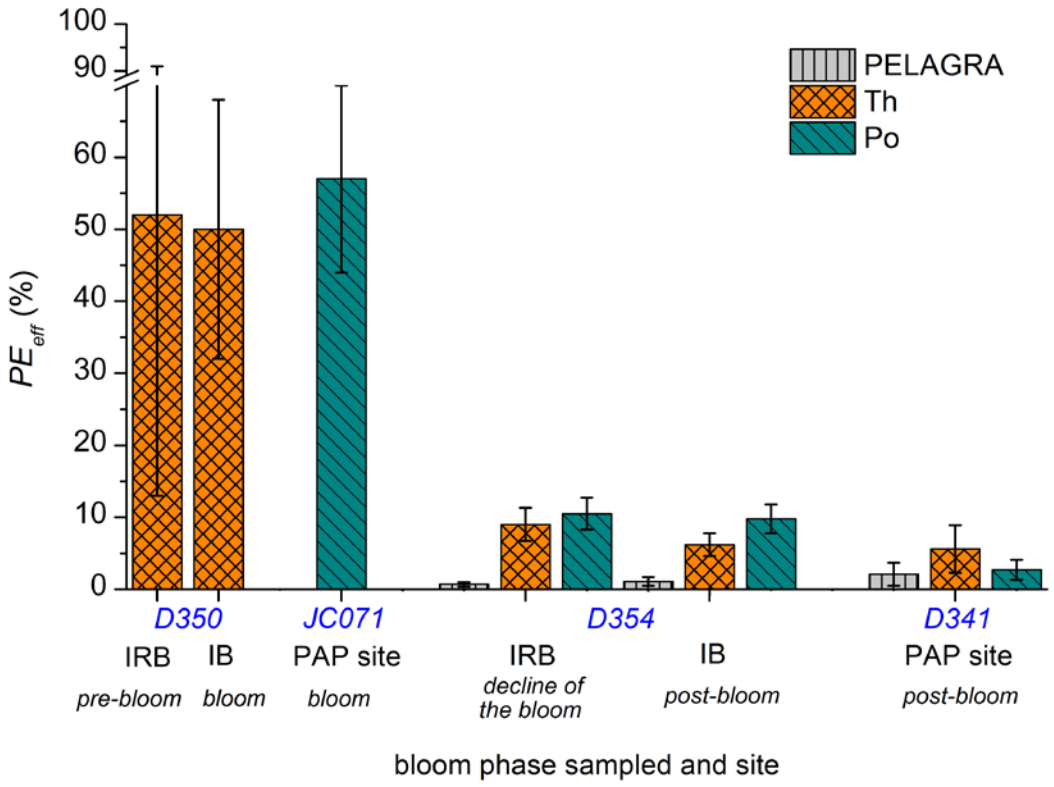

Figure 5. Averaged PE_{eff} (POC flux at MLD + 110 m relative to PP) values (with one standard deviation of the spatial average) during cruises D350 and D354 in both the IRB and IB, and during D341 and JC071 at the PAP site, obtained for PeE_i, ThE_i and PoE_i as a function of the relative timing of sampling and the sampling region. Results from 4 different cruises were employed in order to analyze the seasonal variability in PE_{eff}.

Table S1. Station ID, sampling dates, positions and depth ranges for samples taken in both basins for ^{234}Th measurements during cruise D350. Also detailed by station, with associated uncertainties, are Th fluxes, POC:Th ratios measured by SAPS for large (> 53 μm) and small size particles (1-53 μm) and Th-derived POC fluxes calculated using only large particle data integrated at MLD + 110 m .

	Station ID	Sampling date	Latitude (°N)	Longitude (°W)	Depth range for ^{234}Th (m)	Number of samples for ^{234}Th	Th flux (150 m) (dpm m^{-2} d^{-1})	POC:Th (150 m) (μmol dpm^{-1}) (> 53 μm)	POC:Th (150 m) (μmol dpm^{-1}) (1- 53 μm)	Th-POC (mmol m^{-2} d^{-1})
IRB	2	01/05/2010	60º58'78''	34º59'27''	10-400	10	2474 ± 618	12 ± 7	5.3 ± 0.9	30 ± 17
	3	02/05/2010	60º01'40''	34º57'61''	10-400	10	2921 ± 599	13 ± 9	6.6 ± 2.4	38 ± 21
	4	03/05/2010	60º00'17''	31º58'82''	10-300	10	1108 ± 684	8 ± 7	5.9 ± 0.9	9 ± 7
IB	5	04/05/2010	59º59'41''	28º59'73''	10-300	10	1268 ± 582	14 ± 15	5.5 ± 2.4	17 ± 12
	6	05/05/2010	59º56'65''	26º12'67''	10-400	10	1544 ± 609	9 ±14	4.0 ± 1.6	14 ± 9
	7	06/05/2010	60º50'78''	21º45'06''	10-600	10	1662 ± 562	14 ± 32	3.3 ± 0.8	23 ± 14
	8	07/05/2010	61º59'95''	19º59'96''	10-400	10	1276 ± 708	25 ± 12	5.4 ± 2.7	32 ± 24

Table S2. Station ID, sampling dates, positions and depth ranges for samples taken in both basins for ^{234}Th measurements during cruise D354. Also detailed by station, with associated errors, are Th fluxes, POC:Th ratios measured by SAPS for large (> 53 μm) and small size particles (1-53 μm) and Th-derived POC fluxes calculated using only large particle data integrated at MLD + 110 m . Stations without results for some of the variables are denoted by nan.

	Station ID	Sampling date	Latitude (°N)	Longitude (°W)	Depth range for ^{234}Th (m)	Number of samples for ^{234}Th	Th flux (150 m) (dpm m^{-2} d^{-1})	POC:Th (150 m) (μmol dpm^{-1}) (> 53 μm)	POC:Th (150 m) (μmol dpm^{-1}) (1- 53 μm)	Th-POC (mmol m^{-2} d^{-1})
IB	02	11/07/2010	60º00'09''	19º59'90''	10-400	10	nan	7.3 ± 0.6	4.3 ± 0.3	nan
	04	13/07/2010	61º48'68''	21º02'38''	10-400	10	1210 ± 514	8.1 ± 1.0	2.8 ± 0.3	10 ± 4
	06	15/07/2010	60º00'07''	23º37'70''	10-300	10	1604 ± 435	3.9 ± 0.8	1.8 ± 0.1	6.3 ± 2.1
	27	03/08/2010	62º06'56''	24º18'56''	10-400	10	2139 ± 1000	5.8 ± 0.9	6.2 ± 0.5	12 ± 7
	28	04/08/2010	61º15'48''	20º45'84''	10-400	10	1398 ± 486	6.4 ± 0.8	6.1 ± 0.5	8.9 ± 3.3

	31	05/08/2010	61º55’15’’	26º16’63’’	10-500	10	nan	nan	nan	nan
	33	07/08/2010	60º18’19’’	20º58’67’’	10-400	10	1250 ± 509	6.5 ± 0.4	4.8 ± 0.7	8.1 ± 3.2
IRB	08	17/07/2010	60º00’25’’	34º59’46’’	10-300	10	1710 ± 108	7.5 ± 0.9	4.9 ± 0.4	13 ± 2
	10	19/07/2010	59º56’48’’	41º24’32’’	10-400	10	1859 ± 486	5.4 ± 1.4	3.1 ± 0.2	10 ± 4
	15	21/07/2010	59º59’53’’	34º59’31’’	10-600	10	1962 ± 176	3.0 ± 0.2	3.0 ± 0.4	5.8 ± 1.7
	16	22/07/2010	63º00’01’’	34º59’70’’	10-400	10	1408 ± 386	3.5 ± 0.3	3.3 ± 0.4	5.0 ± 1.4
	18	24/07/2010	62º59’08’’	29º54’13’’	10-400	10	2644 ± 445	4.8 ± 0.5	3.3 ± 0.3	13 ± 2
	20	26/07/2010	58º08’32’’	35º02’12’’	10-400	10	1728 ± 505	7.5 ± 0.5	3.3 ± 0.4	13 ± 4
	22	28/07/2010	63º49’46’’	35º05’51’’	10-400	10	1538 ± 426	4.4 ± 1.0	2.0 ± 0.1	6.7 ± 2.5
	24	01/08/2010	62º28’43’’	28º21’86’’	20-500	10	4447 ± 323	5.7 ± 0.3	3.3 ± 0.3	26 ± 13

Table S3. Station ID, sampling dates, positions and depth ranges for samples taken in both basins for ^{210}Po measurements during cruise D354. Also detailed by station, with associated errors, are Po fluxes, POC:Po ratios measured by SAPS for large (> 53 µm) and small size particles (1-53 µm) and Po-derived POC fluxes calculated using only large particle data integrated at MLD + 110 m.

	Station ID	Sampling date	Latitude (°N)	Longitude (°W)	Depth range for ^{210}Po/^{210}Pb (m)	Number of samples for ^{210}Po/^{210}Pb	Po flux (150 m) (dpm m^{-2} d^{-1})	POC:Po (150 m) (µmol dpm^{-1}) (> 53 µm)	POC:Po (150 m) (µmol dpm^{-1}) (1-53 µm)	Po-POC (mmol m^{-2} d^{-1})
IB	02	11/07/2010	60º00’09’’	19º59’90’’	10-800	13	65 ± 35	84 ± 14	94 ± 16	5.5 ± 1.0
	04	13/07/2010	61º48’68’’	21º02’38’’	10-1000	13	135 ± 35	71 ± 13	62 ± 10	9.6 ± 1.9
	06	15/07/2010	60º00’07’’	23º37’70’’	10-600	10	109 ± 52	88 ± 14	74 ± 11	9.7 ± 2.2
	27	03/08/2010	62º06’56’’	24º18’56’’	10-1000	11	100 ± 52	135 ± 18	417 ± 57	14 ± 2
	28	04/08/2010	61º15’48’’	20º45’84’’	10-500	10	122 ± 54	114 ± 34	200 ± 28	14 ± 4
	31	05/08/2010	61º55’15’’	26º16’63’’	10-500	10	115 ± 82	119 ± 18	124 ± 21	14 ± 2
	33	07/08/2010	60º18’19’’	20º58’67’’	10-2000	12	130 ± 35	187 ± 31	127 ± 17	24 ± 4
IRB	08	17/07/2010	60º00’25’’	34º59’46’’	10-600	10	49 ± 21	66 ± 10	81 ± 13	3.3 ± 0.6
	10	19/07/2010	59º56’48’’	41º24’32’’	10-500	10	92 ± 31	69 ± 11	88 ± 11	6.4 ± 1.0

	15	21/07/2010	59º59'53''	34º59'31''	10-600	10	116 ± 32	102 ± 13	112 ± 13	12 ± 2
	16	22/07/2010	63º00'01''	34º59'70''	10-1500	11	93 ± 45	132 ± 30	130 ± 22	12 ± 3
	18	24/07/2010	62º59'08''	29º54'13''	10-500	12	108 ± 43	122 ± 16	91 ± 12	13 ± 2
	20	26/07/2010	58º08'32''	35º02'12''	10-2150	14	124 ± 51	120 ± 19	77 ± 11	15 ± 3
	22	28/07/2010	63º49'46''	35º05'51''	10-1000	13	73 ± 32	69 ± 11	58 ± 7	5.1 ± 0.8
	24	01/08/2010	62º28'43''	28º21'86''	20-700	10	103 ± 36	111 ± 14	100 ± 106	11 ± 2

Table S4. Station ID, SAPS sampling details and POC and ^{234}Th fractions measured in SAPS for large (> 53 μm) and small size particles (1-53 μm) for cruise D350.

	Station ID	Sampling date	Depth (m)	POC (μmol L^{-1}) $x10^{-3}$ (> 53 μm)	POC (μmol L^{-1}) $x10^{-3}$ (1- 53 μm)	^{234}Th (dpm L^{-1}) $x10^{-3}$ (>53 μm)	^{234}Th (dpm L^{-1}) $x10^{-3}$ (1-53 μm)
IRB	2	01/05/2010	50	264 ± 32	277 ± 70	15 ± 1	43 ± 8
			150	223 ± 19	217 ± 54	19 ± 1	41 ± 7
	3	02/05/2010	50	334 ± 46	275 ± 87	16 ± 1	43 ± 9
			150	244 ± 24	190 ± 98	19 ± 1	29 ± 10
	4	03/05/2010	60	867 ± 63	413 ± 66	111 ± 5	65 ± 7
			160	105 ± 13	229 ± 51	13 ± 1	40 ± 6
IB	5	04/05/2010	50	nan	nan	15 ± 2	43 ± 8
			150	124 ± 19	90 ± 58	9 ± 1	16 ± 8
	6	05/05/2010	50	482 ± 10	39 ± 69	52 ± 8	29 ± 4
			150	92 ± 21	96 ± 56	10 ± 2	24 ± 10
	7	06/05/2010	50	194 ± 12	372 ± 151	21 ± 9	32 ± 10
			150	95 ± 32	109 ± 41	7 ± 1	34 ± 9
	8	07/05/2010	50	35 ± 4	28 ± 6	38 ± 3	10 ± 2
			150	52 ± 14	61 ± 12	2 ± 4	11 ± 2

Table S5. Station ID, SAPS sampling details and POC, ^{234}Th and ^{210}Po and ^{210}Pb fractions measured in SAPS for large (> 53 µm) and small size particles (1-53 µm) for cruise D354.

	Station ID	Sampling date	Depth (m)	POC (µmol L^{-1}) $x10^{-3}$ (> 53 µm)	POC (µmol L^{-1}) $x10^{-3}$ (1- 53 µm)	^{234}Th (dpm L^{-1}) $x10^{-3}$ (>53 µm)	^{234}Th (dpm L^{-1}) $x10^{-3}$ (1-53 µm)	^{210}Po (dpm L^{-1}) $x10^{-3}$ (>53 µm)	^{210}Po (dpm L^{-1}) $x10^{-3}$ (1-53 µm)	^{210}Pb (dpm L^{-1}) $x10^{-3}$ (>53 µm)	^{210}Pb (dpm L^{-1}) $x10^{-3}$ (1-53 µm)
IB	02	11/07/2010	50	392 ± 20	195 ± 9	115 ± 7	164 ± 6	1.6 ± 0.3	3.3 ± 0.4	3.9 ± 0.4	4.8 ± 0.4
			150	167 ± 8	145 ± 7	23 ± 2	33 ± 1	2.0 ± 0.3	3.7 ± 0.5	2.1 ± 0.2	2.4 ± 0.3
	04	13/07/2010	50	129 ± 6	149 ± 8	26 ± 9	47 ± 7	3.0 ± 0.3	1.7 ± 0.3	1.7 ± 0.2	2.1 ± 0.2
			150	114 ± 6	184 ± 9	14 ± 2	65 ± 7	1.6 ± 0.3	5.7 ± 0.8	2.3 ± 0.3	3.3 ± 0.4
	06	15/07/2010	40	480 ± 24	462 ± 23	110 ± 4	81 ± 5	1.7 ± 0.3	2.5 ± 0.4	5.0 ± 0.4	6.7 ± 0.4
			140	132 ± 7	127 ± 06	34 ± 6	71 ± 4	1.5 ± 0.2	3.6 ± 0.4	2.4 ± 0.3	2.6 ± 0.3
	27	03/08/2010	50	705 ± 35	485 ± 24	85 ± 9	25 ± 2	1.6 ± 0.3	1.3 ± 0.3	6.7 ± 0.6	3.0 ± 0.4
			150	311 ± 16	656 ± 32	54 ± 8	106 ± 6	2.3 ± 0.3	8.3 ± 0.9	3.3 ± 0.3	5.6 ± 0.4
	28	04/08/2010	40	465 ± 23	516 ± 26	67 ± 5	76 ± 5	2.4 ± 0.3	2.2 ± 0.3	4.8 ± 0.4	3.7 ± 0.3
			140	458 ± 22	487 ± 25	284 ± 1	80 ± 6	1.6 ± 0.4	2.1 ± 0.2	2.3 ± 0.5	5.6 ± 0.5
			400	390 ± 39	nan	11 ± 2	nan	2.1 ± 0.3	1.7 ± 0.2	1.7 ± 0.2	2.5 ± 0.3
	31	05/08/2010	50	242 ± 12	242 ± 12	nan	nan	3.1 ± 0.3	1.7 ± 0.2	1.7 ± 0.2	3.5 ± 0.3
			150	288 ± 14	385 ± 19	nan	nan	2.4 ± 0.3	2.0 ± 0.3	4.1 ± 0.4	2.5 ± 0.3
	33	07/08/2010	50	345 ± 17	333 ± 17	28 ± 2	110 ± 1	2.2 ± 0.3	5.1 ± 0.8	2.0 ± 0.3	4.5 ± 0.5
			150	206 ± 10	275 ± 14	32 ± 1	57 ± 7	1.1 ± 0.2	1.6 ± 0.3	1.7 ± 0.2	2.8 ± 0.3
			400	180 ± 18	140 ± 14	10 ± 2	15 ± 2	1.0 ± 0.2	2.1 ± 0.3	3.6 ± 0.4	1.3 ± 0.2
IRB	08	17/07/2010	50	293 ± 15	583 ± 29	89 ± 6	168 ± 5	3.0 ± 0.4	3.0 ± 0.5	4.8 ± 0.5	4.2 ± 0.5
			150	99 ± 5	86 ± 43	13 ± 5	18 ± 3	1.5 ± 0.2	1.0 ± 0.2	2.3 ± 0.3	3.8 ± 0.4
	10	19/07/2010	50	552 ± 28	562 ± 28	94 ± 5	174 ± 4	4.0 ± 0.4	4.1 ± 0.4	4.7 ± 0.4	9.7 ± 0.5
			150	192 ± 10	353 ± 18	35 ± 9	115 ± 4	2.8 ± 0.4	4.0 ± 0.4	2.2 ± 0.2	5.4 ± 0.4

	15	21/07/2010	50	480 ± 24	604 ± 30	71 ± 7	181 ± 5	2.5 ± 0.4	5.7 ± 0.5	4.6 ± 0.4	4.6 ± 0.3
			150	360 ± 18	356 ± 18	122 ± 6	120 ± 5	3.5 ± 0.4	3.2 ± 0.3	4.6 ± 0.3	5.5 ± 0.4
	16	22/07/2010	40	206 ± 10	408 ± 20	86 ± 8	149 ± 6	4.5 ± 0.6	2.6 ± 0.4	4.1 ± 0.5	6.0 ± 0.6
			140	100 ± 5	310 ± 15	29 ± 6	94 ± 9	7.6 ± 0.2	2.4 ± 0.4	3.5 ± 0.4	3.6 ± 0.4
	18	24/07/2010	40	767 ± 38	451 ± 23	56 ± 5	55 ± 3	4.5 ± 0.6	2.8 ± 0.4	5.3 ± 0.6	6.2 ± 0.5
			140	357 ± 18	282 ± 14	75 ± 6	86 ± 5	3.0 ± 0.4	3.1 ± 0.4	3.6 ± 0.3	3.2 ± 0.3
	20	26/07/2010	50	492 ± 25	730 ± 36	32 ± 4	135 ± 7	1.7 ± 0.4	4.4 ± 0.6	2.6 ± 0.4	6.7 ± 0.6
			150	189 ± 94	197 ± 98	26 ± 4	59 ± 6	1.6 ± 0.3	2.6 ± 0.3	2.1 ± 0.2	2.5 ± 0.3
			400	210 ± 21	250 ± 25	12 ± 2	7.6 ± 0.2	1.6 ± 0.2	2.2 ± 0.3	1.5 ± 0.2	1.7 ± 0.2
	22	28/07/2010	50	341 ± 17	477 ± 24	58 ± 8	320 ± 6	2.7 ± 0.3	3.2 ± 0.4	4.4 ± 0.4	3.5 ± 0.3
			200	123 ± 62	237 ± 12	28 ± 6	116 ± 5	1.8 ± 0.3	4.1 ± 0.5	2.3 ± 0.3	3.8 ± 0.3
			400	310 ± 31	180 ± 18	21 ± 2	38 ± 2	4.7 ± 0.6	6.0 ± 0.7	4.9 ± 0.5	5.3 ± 0.5
	24	01/08/2010	40	491 ± 25	571 ± 29	122 ± 7	182 ± 6	3.0 ± 0.3	2.8 ± 0.3	4.3 ± 0.3	6.0 ± 0.3
			140	276 ± 14	326 ± 16	48 ± 5	96 ± 9	2.5 ± 0.3	3.2 ± 0.3	3.7 ± 0.3	4.3 ± 0.3

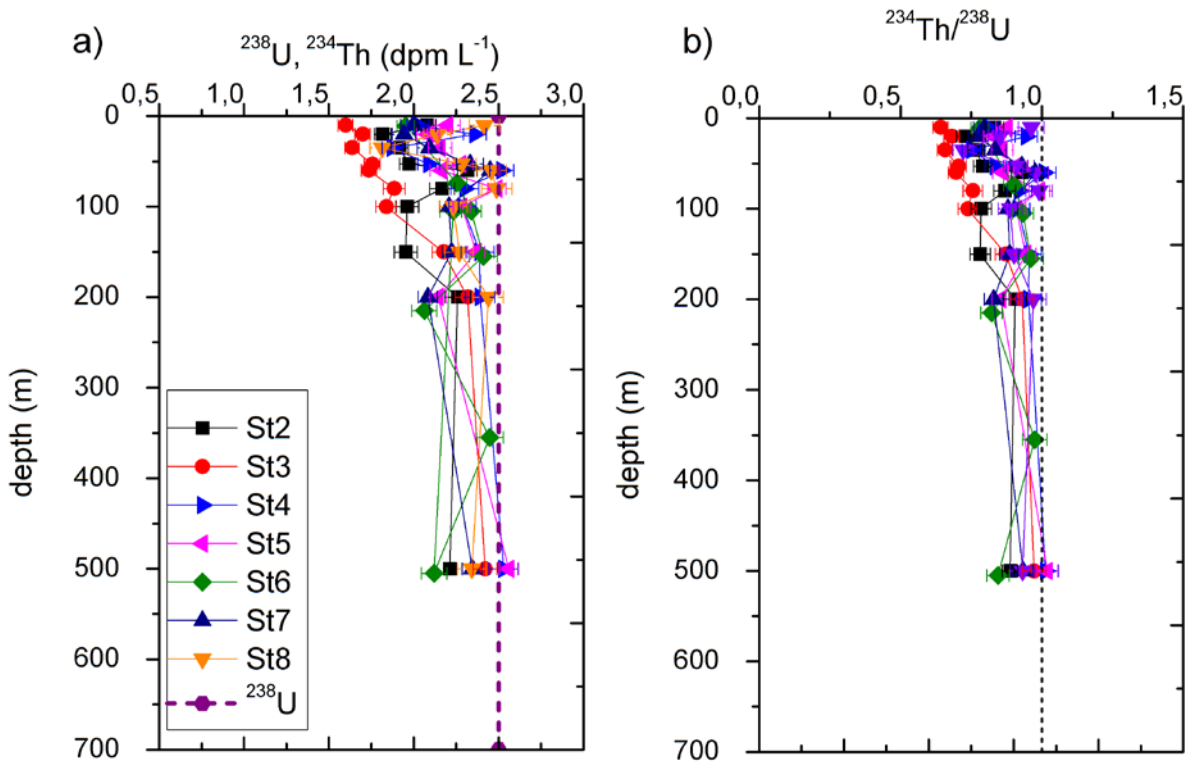

Figure S1. (a) ^{234}Th activity (in dpmL^{-1}) and (b) ^{234}Th/^{238}U ratio versus depth for cruise D350. Symbols are given in panel (a) of the figure.

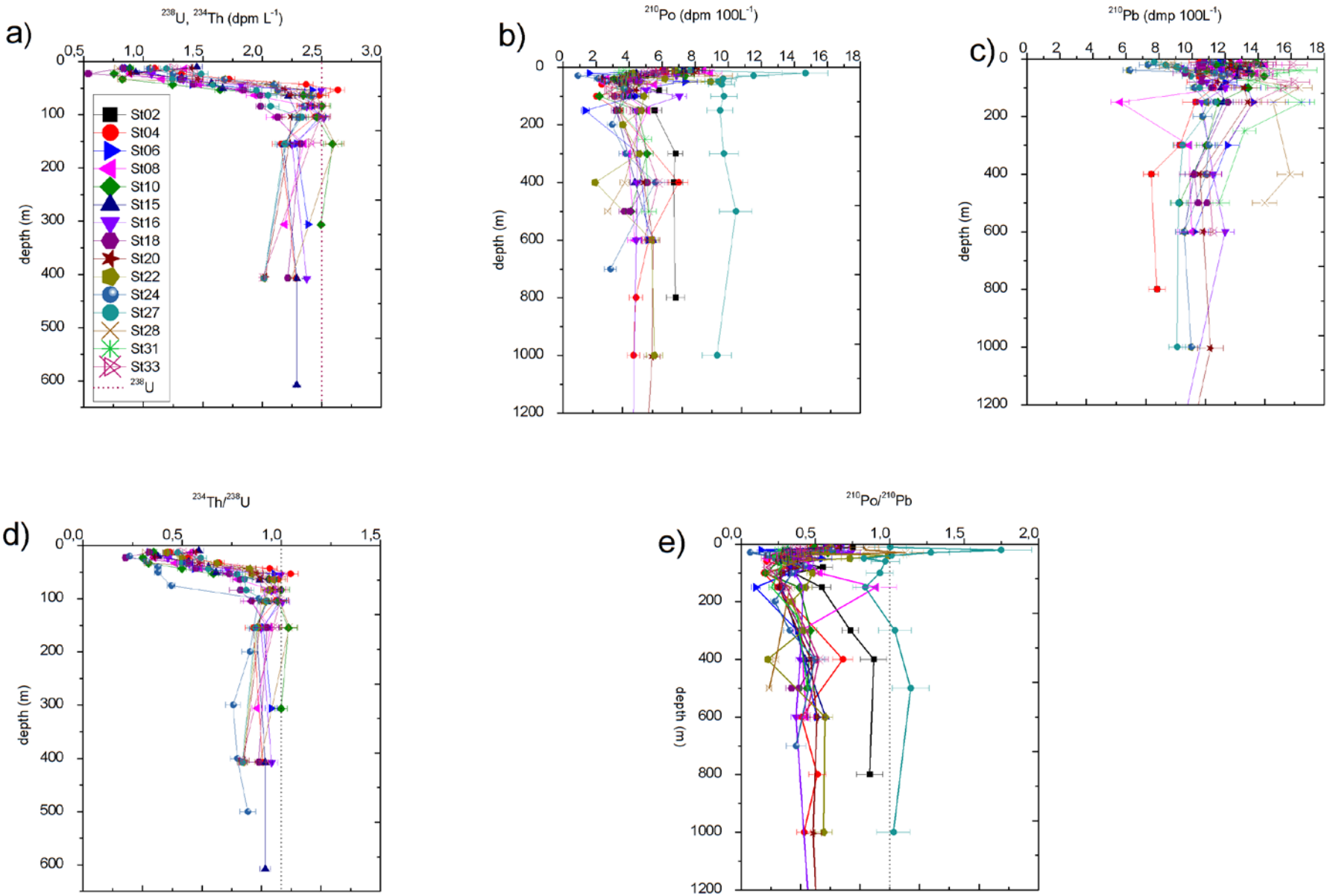
a)
^{238}U, ^{234}Th (dpm L^{-1})
depth (m)
St02
St04
St06
St08
St10
St15
St16
St18
St20
St22
St24
St27
St28
St31
St33
^{238}U
b)
^{210}Po (dpm 100L^{-1})
depth (m)
c)
^{210}Pb (dmp 100L^{-1})
depth (m)
d)
^{234}Th/^{238}U
depth (m)
e)
^{210}Po/^{210}Pb
depth (m)

Figure S2. (a) ^{234}Th activity (in dpmL^{-1}), (b) ^{210}Po activity (in dpm100L^{-1}), (c) ^{210}Pb activity (in dpm100L^{-1}), (d) ^{234}Th/^{238}U ratio and (e) ^{210}Po/^{210}Pb ratios versus depth for cruise D354. Symbols are given in panel (a) of the figure.